Concept of NICA Collider

NICA/MPD project leaders A.Sisakian, V.Kekelidze, A.Sorin

NICA project working group
E.Ahmanova[1], A.Eliseev[1], Yu.Filatov[1], T.Katayama[2], A.Kuznetsov[1], H.Khodzhibagiyan[1], S.Kostromin[1], O.Kozlov[1], O.Kunchenko[1], V.Lebedev[3], V.Mikhailov[1], I.Meshkov[1], V.Monchinsky[1], E.Muravieva[1], S.Nagaitsev[3], A.Philippov[1], R.Pivin[1], A.Sidorin[1], A.Smirnov[1], N.Topilin[1], G.Trubnikov[1], Yu.Tumanova[1], S.Yakovenko[1], P.Zenkevich[4],

1 – JINR, 2 – retired from Tokyo University, 3 – FNAL, 4 - ITEP

Editor I.Meshkov

JINR, DDubna

January 2010

Contents

1. Introduction

The goal of the NICA project, as formulated in the Conceptual Design Report (CDR) [1.1], is construction at JINR of the new accelerator facility that consists of
- cryogenic heavy ion source KRION of Electron String Ion Source (ESIS) type,
- source of polarized protons and deuterons,
- the "old" linac LU-20,
- a new heavy ion linear RFQ accelerator,
- a new superconducting Booster-synchrotron (that will be placed inside of the yoke of the decommissioned Synchrophasotron),
- the existing superconducting heavy ion synchrotron Nuclotron (being developed presently to match the project specifications),
- collider having two new superconducting storage rings,
- new set of transfer channels.

General attention in this report is devoted to the heavy ion collision mode of the collider operation.

The facility will have to provide ion-ion and ion-proton collisions in energy range of 1 ÷ 4.5 GeV/u and collisions of polarized proton-proton (5 ÷ 12.6 GeV) and deuteron-deuteron (2 ÷ 5.8 GeV/u) beams. Correspondingly, we consider two acceleration and stacking chains of heavy ions and polarized protons and deuterons:

1) Electron string ion source → RFQ-linac → Booster → Nuclotron → Collider
2) Source of polarized ions (or protons)→ Nuclotron → Collider

Collider will be operated at a fixed energy without acceleration of an injected beam. The collider will have two interaction points (IP). The MultiPurpose Detector (MPD) located in one of IP, is aimed for experimental study of hot and dense strongly interacting matter and search for possible manifestation of signs of the mixed phase and critical endpoint in heavy ion collisions. The second IP is used for the Spin Physics Detector (SPD). Concept of the MPD design is described in [1.2], the SPD design is in progress.

To cover the required range of the beam energy the maximum magnetic rigidity of the collider rings has to be of 45 T·m, that is equal to the Nuclotron one. In the CDR the version of the collider location inside existing experimental building #205 was described. The building size permits to place a ring of maximum circumference of about 250 m. In order to have the collider magnetic rigidity of 45 T·m and sufficient space for long straight sections the field of the bending magnets has to be of about 4 T. Preliminary design of such magnets has been performed, however main problem to be solved is to form the field of required quality in a short curved magnet, that requires a long R&D stage.

Collider 2T

Very attractive alternative is to use for the collider magnetic system with the "Nuclotron-type" magnets [1.3]. The Nuclotron superconducting (SC) magnets are based on a cold-iron window frame type yoke and low inductance winding made of a hollow composite superconductor. The field geometry is formed by the iron yoke. The main elements of the Nuclotron, including SC magnetic system, have been fabricated by the machinery workshops of The Laboratory for High Energy of JINR without involving specialized industry. This work has brought a great experience to the Institute staff in the field of SC magnet design and manufacturing. Such type of magnets is planed to be used for construction of SIS-100 synchrotron of the FAIR project and for

the NICA Booster. Preliminary design of the magnets for NICA Booster and Collider is done already and construction of the prototypes is scheduled for 2010 (see Section 8 below).

The bending field in the iron-dominated magnets is limited by the value of about 2 T. In this case the collider circumference has to be of 300 – 400 m to provide required magnetic rigidity and provide sufficient room for detectors and insertion devices. This requirement can be met when the collider rings are located across the reconstructed experimental building #205 as it shown in Fig. 1.1, 1.2. In accordance with this scheme the long straight sections of the collider (containing the IPs) are situated inside the building and two arcs with the bending magnets are placed in the especially built concrete tunnels ("corridors").

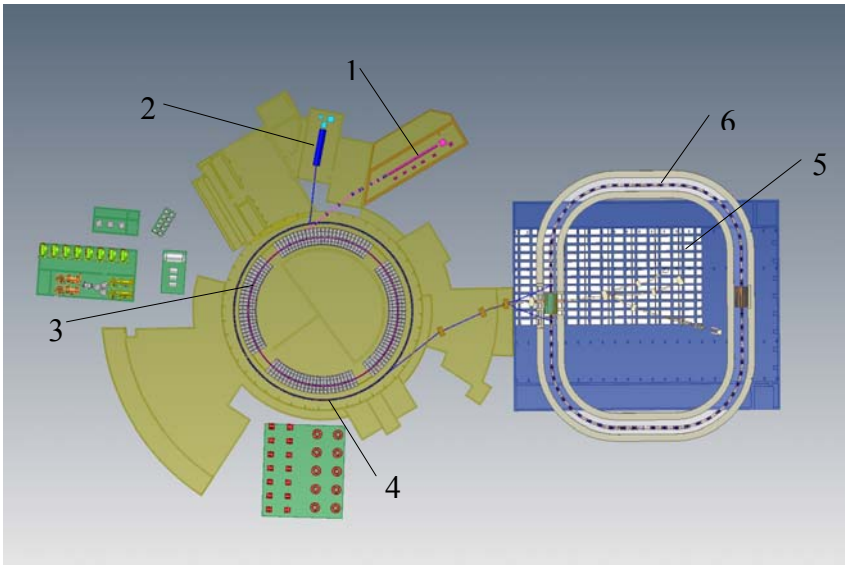

Fig. 1.1. Scheme of the NICA facility: 1 - ESIS source and new RFQ linac, 2 – polarized beam source and LU-20; 3 – Booster, 4 – Nuclotron, 5 – existing experimental building #205, 6 – collider rings;

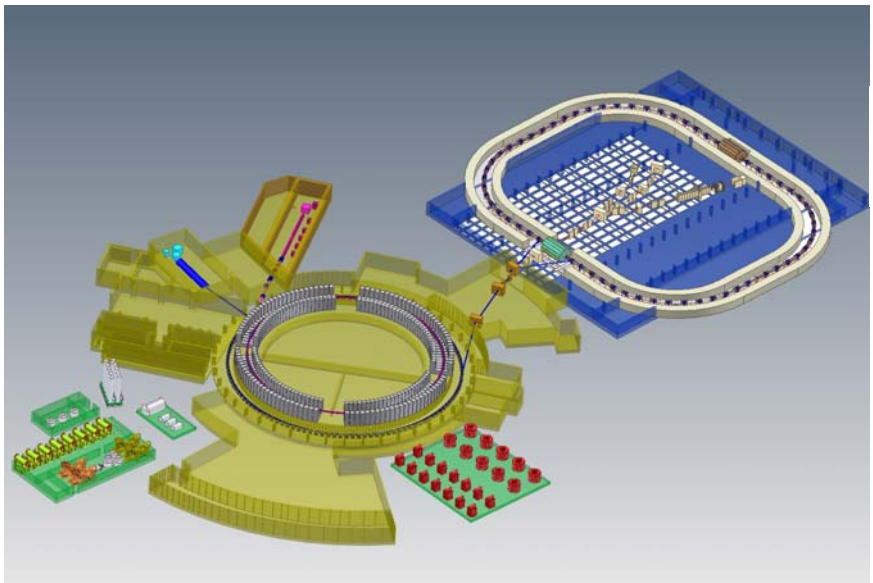

Fig. 1.2.Layout of the NICA facility

At this version the LHEP working area geometry allows to construct collider rings (with required radiation shielding) of the circumference between 340 and 380 m. Both detectors will be located in convenient places of the experimental building #205 that simplifies their test and final assembling. Central part of the building hall will be used for fixed target experiments. Maximum length of the long straight sections of the collider can be about 50 m that seems to be long

enough for placement of the detectors, providing the beam superposition and separation. One of the long straight sections will be used for the beam injection, the other – for spin control devices.

Taking into account all these advantages the *"Collider 2T"* version was chosen as the base line for further design of the NICA facility. *This decision was taken December 3, 2009.*

In this report we present the concept and first technical solutions for the Collider 2T.

Injection chain and ion storage
The parameters of the injection chain (Fig. 1.3) and the facility working cycle are presented in the CDR [1.1] and they do not depend significantly on the collider design.

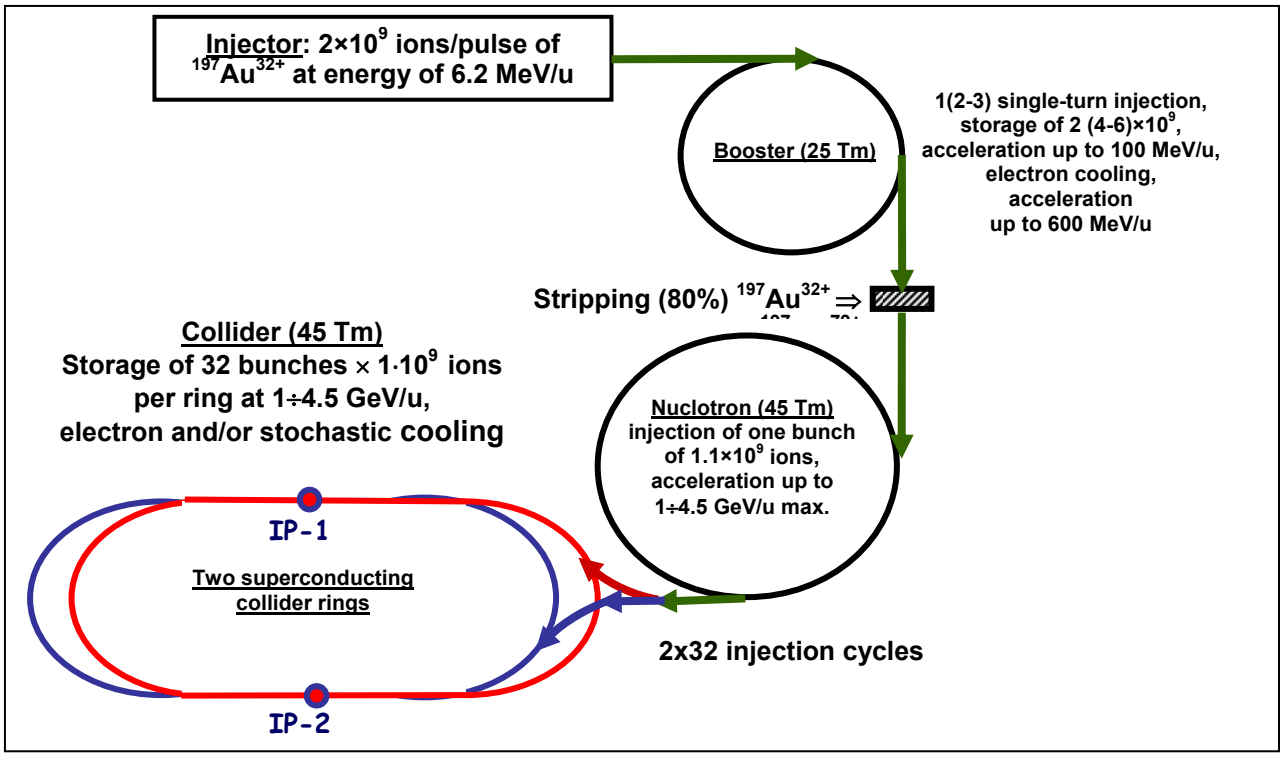

Fig. 1.3. Scheme and general parameters of the NICA injection chain

The injection cycle duration lasts 5 sec. approximately. Therefore beam storage time in the collider requires about 5.5 min. Ion storage in the collider rings are performed with barrier buckets technique and stochastic or electron cooling application (Chapter 6).

In NICA CDR [1.1] we proposed the ion storage scheme based on preparation of short bunches of necessary parameters in Nuclotron at the end of acceleration and before extraction. Then the formed bunch is extracted and injected into collider. Such a procedure is repeated necessary number of Nuclotron cycles. The ion beams in Collider rings are stored in form of bunches ready for collisions. This scheme has certain advantage mainly because it uses rather conventional scheme.

General requirements to the collider rings
Large number of superperiods in the ring optic structure is required to provide long polarization life-time at the collisions of polarized beams. Such a lattice structure can be constructed when two collider rings are placed *one upon the other* and the beam superposition/separation is provided in *the vertical plane*. To have a minimal space for the beam superposition/separation in the IP straight sections the distance between the rings median planes has to be as small as possible. That can be achieved with dipole and quadrupole magnets having two apertures in one

yoke. In this report we discuss a preliminary design of *"The twin bore magnets"* that have a distance between apertures of about 30 cm (Chapter 8).

The collider rings have to provide two main different operation modes: heavy ion collisions and collisions of polarized beams.

For *the polarized beams collisions* the required luminosity level (of the order of $10^{30} \div 10^{31}$ $cm^{-2}s^{-1}$) can be achieved relatively easily because of small electric charge of the colliding particles (that diminishes the problems with the beam space charge). General challenges in this mode are to provide long polarization life-time and realize collisions in two regimes: at transverse and at longitudinal polarization at IP. Insertion devices dedicated to the spin control at IP and compatible with the ring optics structure are under design presently. Optimization of the ring optics structure and working point to provide long polarization life time will be performed at further stages of the collider design.

Main problem to be solved in *the heavy ion collision mode* is to achieve the luminosity level of the order of 10^{27} $cm^{-2}s^{-1}$. In the NICA beam energy range it is possible only at the beam emittance corresponding to the space charge limit. We plan to achieve sufficiently small beam emittance with application of stochastic and electron cooling systems. Correspondingly, the ring optics has to be designed in accordance with specific requirements of these systems.

MultiPurpose Detector (MPD)
The MPD consists of different detector subsystems (Fig.1.3) providing an efficient registration of the ion collision products. It occupies 8.14 m of long straight section free space that does not interfere with the task of low beta function formation at IP.

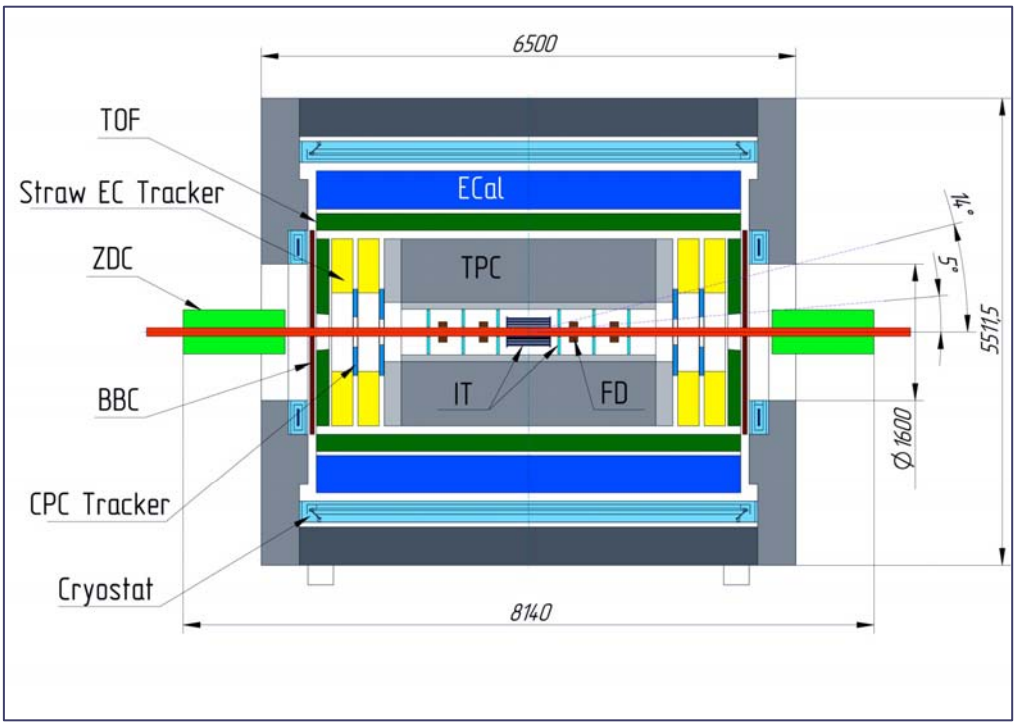

Fig.1.3. Scheme of the MultiPurpose Detector (MPD)
TOF – time of flight, EC – electromagnetic tracker, ZDC – zero degree calorimeter,
TPC – time projection chamber, BBC – beam-beam counter, CPC – charge projection chamber,
IT – inner tracker, FD - forward detector, Cryostat – for SC solenoid of 0.5 T,

The MPD design is optimized for the beam collisions at *zero crossing angle*. Therefore the colliding beams have to be *bunched* and the bunch length has to be short enough to concentrate

the luminosity in the central part of the detector. At the current design MPD acceptance allows to use 80% of the luminosity in its inner tracker if r.m.s. *bunch length is of 30 cm.* The Collider 2T parameters presented in this report meet this requirement. Correspondingly, the RF harmonics number is chosen to provide the bucket length of 1.8 ÷ 2.4 m.

The main effect limiting the luminosity level is *the intrabeam scattering process (IBS)* leading to increase of the beam emittance. To stabilize the bunch parameters the cooling systems have to provide the cooling rates that are not less than the IBS heating rates. To diminish the IBS growth rates the ring has to be operated *below transition energy*. This is preferable also as regards the beam stability. The IBS growth rate for horizontal degree of freedom is larger than for the vertical one. Therefore at equal cooling power for both transverse planes the equilibrium corresponds to a ribbon beam. To provide *collisions of round beams* at the same beta-functions in the horizontal and vertical planes we plan to work in the vicinity of *coupling resonance*. The sources of the coupling in the ring are solenoids of the detector and electron cooling system, the coupling should be regulated by skew qaudrupoles.

The bunch intensity can be limited by different kind of instabilities. To obtain maximum bunch intensity one should presume required chromaticity correction system and application of feed back systems (see Chapter 4 below).

In the equilibrium between IBS and cooling the luminosity life-time is determined mainly by the ion loss due to interaction with residual gas. Vacuum system of the rings is designed to provide the residual gas pressure below 10^{-11} Torr. That corresponds to the ion life-time of about 10 hours. However in presence of the intense ion beam one needs to presume corresponding measures to avoid vacuum instability. Serious attention has to be devoted to the possibility of electron cloud formation and measures to suppress this effect (Chapter 10).

The report structure is chosen to follow some logic. After Introduction (Sec.1) we describe
2) Beam parameters necessary for achievement of the project luminosity.
3) Then the collider rings size and interim version of the ring lattice are presented. This section is followed by
4) Review of beam stability problems
5) IBS related problems, particularly – the lattice optimization for IBS rate decrease,
6) Beam storage with barrier buckets technique, stochastic cooling of coasting beam,
7) Bunched beam formation and stochastic cooling,
8) Consideration given in Sections 2 and 7 allows analyzing requirements on RF system parameters,
8-2) Feasibility of critical energy tuning
9) Hardware – SC magnets
10) Electron cooling and related problems
11) Vacuum, electron clouds, etc.

References

1.1. Conceptual Design Report of Nuclotron-based Ion Collider fAcility (NICA), JINR, 2008
1.2. Conceptual Design Report of MultiPurpose Detector, JINR, 2009
1.3. H.G.Khodzhibagiyan and A.A.Smirnov, The concept of a superconducting magnet system for the Nuclotron, Proc. of the 12th Int. Cryogen. Eng. Conf., 1988, pp. 841–844; A.M.Baldin et al., Superconducting fast cycling magnets of the Nuclotron, IEEE Trans. on Applied Superconductivity, vol. 5, 2 (1995) p. 875–877.

2. Luminosity and the beam parameters

At identical colliding bunches of a round shape of the cross-section the luminosity can be estimated by the following formula:

$$L = \frac{N_b^2}{4\pi\varepsilon\beta^*} F_{coll} f\left(\frac{\sigma_s}{\beta^*}\right), \qquad (2.1)$$

where N_b is the ion number in the bunch, ε is the transverse unnormalized r.m.s. emittance, β^* is the beta function in the interaction point, the collision repetition rate F_{coll} is determined as the bunch number in the ring n divided by the revolution period T_{rev}, the factor

$$f_{HG}\left(\frac{\sigma_s}{\beta^*}\right) = \frac{1}{\sqrt{\pi}} \int_{-\infty}^{\infty} \frac{exp(-u^2)du}{\left[1+\left(\frac{u\sigma_s}{\beta^*}\right)^2\right]} \approx \frac{1}{1+\left(\frac{\sigma_s}{2\beta^*}\right)^2}. \qquad (2.2)$$

is close to unity when the longitudinal rms beam size σ_s is much less than the value of beta function at the interaction point (Fig.2.1). The luminosity decrease with increase of the bunch length is referred as "the hour glass effect". One can see that the approximate function differs insignificantly from exact one.

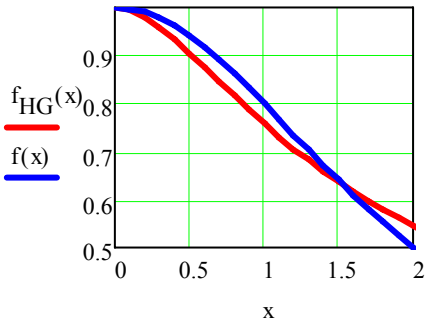

Fig.2.1. "Hour glass effect" function:
exact value $f_{HG}(x)$ (red curve) and approximate one $f(x)$ (2.2) (blue curve),
$x = \sigma_s / \beta^*$

At σ_s = 0.3 m and β^* = 0.5 m the hour glass function f_{HG} = 0.875.

To reach maximum peak luminosity one needs to satisfy the following obvious requirements:

- minimum beta function in the IP;
- maximum collision repetition rate (that corresponds to the maximum bunch number in the rings);
- maximum bunch intensity;
- minimum beam emittance and
- minimum bunch length.

The last requirement is relatively weak because of weak dependence in (3.2). The rms bunch length of about 30 cm motivated by the MPD design makes possible to reduce significantly "the hour glass effect" at reasonably small beta function in the IP. Further decrease of the bunch length leads to increase of the bunch peak current but does not influence on the luminosity practically. Therefore below we discuss *the bunch length equal to 30 cm.*

The proposed scheme of the collider feeding with the heavy ions presumes storage in the collider of a coasting beam initially. After storage of a required ion number an adiabatic bunching is provided on the harmonics number equal to the required bunch number. The beam storage and bunching are realized under support of the stochastic cooling, therefore we can expect that the beam emittance and momentum spread can be prepared as small as necessary. After preparation of the bunch at low RF harmonics the bunch compression will be performed and the bunch of a short length during the collisions will be stabilized in high RF harmonics with electron and stochastic cooling.

Thus for the luminosity estimation we can treat the bunch intensity, number of the bunches, emittance and momentum spread as the parameters that can be optimized independently. In this chapter we discuss briefly the main limitations of these parameters and limitations related to the ring design.

2.1. Lower limit of beta functions in the interaction point

The minimum beta function value is limited by the design of the collider straight section in the vicinity of the interaction point: the beam radius in the lenses of the low beta insertion section has to be small enough for reasonable aperture of the lenses.

Neglecting the influence of the detector magnetic field on the particle motion, the dependence of the beta function on the distance from the IP s is given by the formula:

$$\beta(s) = \beta^* + \frac{s^2}{\beta^*}. \qquad (2.3)$$

To avoid the ion losses in the low beta quadrupoles the vacuum chamber aperture a has to be larger than the beam rms radius $\sigma_\perp$: $a = n_\sigma \sigma_\perp$ at n_σ in the range 4 ÷ 6. This gives the following approximate limitation for the β^*:

$$\beta^* > n_\sigma^2 \frac{L_q^2}{a^2} \varepsilon, \qquad (2.4)$$

where ε is unnormalized rms emittance, L_q is the distance from the quadropole lens to the IP. This limitation is sufficient at small ion energy, when the beam emittance has to be large enough to avoid tune shift limitation. Obviously the L_q has to be as small as possible, however it contradicts to other requirements for the collider optics near the IP.

2.2. Collision repetition rate

The collider has to be operated at the bunch number as large as possible. The maximum bunch number is limited by requirement to avoid parasitic collisions in the vicinity of the interaction point. Two possible additional limitations are related to “electron cloud” effect and multibunch instability (Chapters 4 and 10).

One can avoid the parasitic collisions if the interbunch distance is longer than the distance between dipole magnets providing the beam separation in the interaction region. One of the modes of the collider operation presumes the work when magnetic rigidity of the first ring is not equal to the rigidity of the second ring. It is possible in the case when the rings have no common quadrupole lenses. In this case the first dipole of the beam separation system is located at about 4.5 m from the IP (Fig. 2.1, for details see chapter 3). Correspondingly the minimum distance between bunches can be chosen of about 10 ÷ 11 m. Thus the maximum bunch number in each ring of the collider can lie in between 32 and 38, depending on the ring circumference.

At such a design the triplet of the low beta insertion is located at about 10 m from the IP that limits minimum achievable beta function. At the beta function in IP of 0.5 m the maximum beta function in the triplet is equal to about 300 m (Fig. 2.2), and this value is almost inversely proportional to the beta function in the IP.

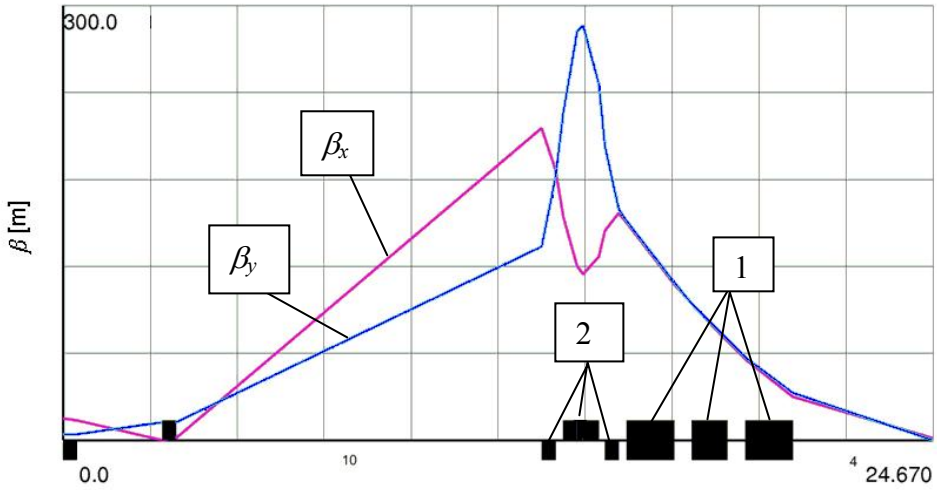

Figure 2.2. Preliminary design of the long straight section and amplitude β-functions in the half of the section. The IP is in the right corner of the graph. $\beta^*=\beta_x = \beta_y = 0.5$ m. 1 – dipole magnets, 2 – low beta quadrupoles.

We assume in the estimations below that the *minimum beta function in the IP is equal to 0.5 m* and the *bunch number n* in each ring is equal to *32*. At maximum experiment energy (that corresponds to minimum emittance at the same tune shift) one can decrease hopefully the beta function to the value of about 20 – 30 cm with corresponding increase of the luminosity.

2.3. Bunch intensity

Strongest limitations of the luminosity related to the space charge effects are *incoherent tune shift* and tune shift related to so called *beam-beam effect*. The incoherent (Lasslet) tune shift for "free" *ion bunch of axially symmetric Gaussian distribution* can be estimated as follows (see details in Chapter 4):

$$\Delta Q = -\frac{Z^2}{A}\cdot\frac{r_N N_b}{4\pi\beta^2\gamma^3\varepsilon}\cdot F_b, \qquad (2.5)$$

where Z and A are the charge and atomic numbers of the ion correspondingly, r_N is the nucleon classical radius, N_b is ion number perbunch, β and γ are the relativistic factors. The bunching factor

$$F_b = \frac{C_{Ring}}{\sqrt{2\pi}\sigma_s} \qquad (2.6)$$

is equal to ratio of peak to mean bunch current (C_{Ring} is the ring circumference, σ_s is r.m.s. bunch length).

For numerical estimates we have taken "the reference parameters" (Table 2.1) corresponding to the peak luminosity of

$$L_{peak} \approx 1 \cdot 10^{27}\ \mathrm{cm}^{-2} \cdot \mathrm{s}^{-1}.$$

Table 2.1. The "reference" parameters of the collider

Energy, GeV/u	3.5
Ring circumference, m	336
Betatron tunes	7.6
Transition energy, GeV/u	4.9
Ion number per bunch	1e9
Rms unnormalized beam emittance ε_{un}, π·mm·mrad	0.34
Rms momentum spread σ_p	1e-3
Rms bunch length σ_s, m	0.3
Number of bunches	32
Number of RF harmonics	160
Lasslett tune shift (2.5)	0.05

The limitation specific for colliders is related to so called *beam-beam effect* – scattering of particles of one beam in electromagnetic field of the encounter (another) beam. It leads to formation of a betatron tune shift. The linear part of this tune shift (so called "*beam-beam parameter*") for the axially symmetric Gaussian bunched beam is equal to

$$\xi = \frac{Z^2 r_p}{A} \frac{N_b}{4\pi\beta^2\gamma\varepsilon} \frac{1+\beta^2}{2}. \qquad (2.7)$$

At the NICA parameters this value is less than Lasslet tune shift by one order of magnitude, at least, in the total experiment energy range at constant bunch parameters (Fig. 2.3).

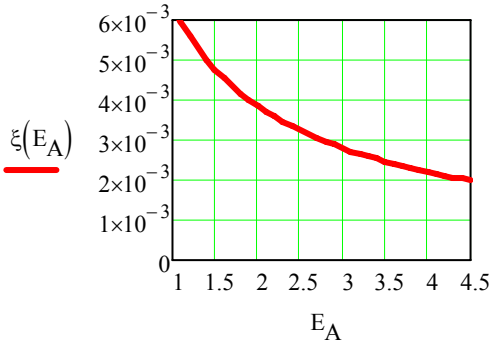

Fig.2.3. Beam-beam parameter vs ion energy
for bunch parameters listed in Table 2.1.

If the luminosity is limited by the tune shift value ΔQ_{max} and ion number per bunch N_b is const (the same at any energy), one can express the Formula for luminosity as follows:

$$L = \Delta Q_{max} \cdot \beta^3\gamma^3 \cdot \frac{A}{Z^2 r_N} \cdot \frac{n N_b c}{C_{Ring}^2} \cdot \frac{\sqrt{2\pi}\sigma_s}{\beta^*} \cdot f_{HG}\left(\frac{\sigma_s}{\beta^*}\right). \qquad (2.8)$$

At constant tune shift the luminosity is proportional to the bunch intensity N_b and is scaled with the energy as $\beta^3\gamma^3$.

If ΔQ_{max} and N_b are kept constant with energy variation it assumes corresponding variation of beam emittance (see (2.5)):

$$\varepsilon \propto \frac{1}{\beta^2 \gamma^3 |\Delta Q|} \ . \tag{2.9}$$

The evolution of L_{peak} (2.8) and beam emittance ε (2.9) with energy (Fig. 2.4) shows that the reference parameters values do allow us to reach the required luminosity $1 \cdot 10^{27}$ cm^{-2}·s^{-1} at ion energy of 3.5 GeV/u.

Moreover, the luminosity exceeds this level significantly at E_{ion} > 3.5 GeV/u. At the same time, it decreases drastically with ion energy reduction below 3.5 GeV/u. Therefore, the task of the project development was to find out which reserves could be used for luminosity increase in the low energy range.

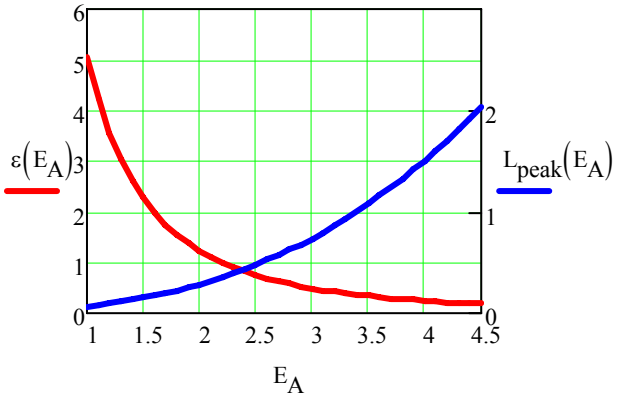

Fig. 2.4. Peak luminosity and beam emittance vs ion energy;
blue curve and right axis – luminosity [10^{27} cm^{-2}·s^{-1}],
red curve and left axis – emittance [π·mm·mrad]

An evident way for this purpose is an increase the ion number per bunch at constant ΔQ value (see (2.8)). Generally speaking, one more strong effect comes into play with bunch intensity increase – intrabeam scattering (IBS). However, its rates even decrease with N_b growth if we keep ΔQ = const by increase of the bunch emittance. Indeed, the IBS rates are scaled with the ion number and emittance approximately as

$$\frac{1}{\tau_{IBS}} \propto \frac{N_b}{\varepsilon^2} \Rightarrow \frac{\Delta Q^2}{N_b} . \tag{2.10}$$

So, if we increase $N_b \Rightarrow$ 5e9 the luminosity at 1 GeV/u becomes equal to 0.3e27 cm^{-2}·s^{-1} and emittance has to be increased up to 25 π·mm·mrad (!).

More detailed analyses is presented in concluding Chapter 12.

Other effects limiting the peak bunch current are *single bunch coherent instabilities*. The most important among them are (see Chapter 4)

1) Longitudinal and transverse microwave instabilities (similar to coasting beam ones).
2) Longitudinal and transverse coupling mode instabilities.
3) Strong and weak head –tail instabilities and multi-bunch instabilities.

Preliminary consideration of these effects (Chapter 4) showed that the longitudinal microwave instability below the critical energy has no importance if the chamber impedance is much less than the longitudinal space charge impedance (at the NICA parameters it is valid if the longitudinal chamber impedance is about a few Ohm). The transverse microwave instability can be suppressed too for moderate momentum spread (about 0.1%). However coupling mode instabilities and weak head-tail could be dangerous if we are going to work near transition energy. Correspondingly it is necessary to design the *chromaticity correction system* for suppressing weak head-tail.

The beam stability problem requires very careful study for the NICA parameters because of relatively large peak current and low beam energy. On the basis of preliminary estimations, in this report we assume that adequate measures will allow stabilizing the bunch at the ion number of

$$N_b \sim (1 \div 2)\cdot 10^9. \qquad (2.11)$$

2.4. The bunch momentum spread and the ring momentum slippage factor

The bunch momentum spread does not influence directly on the luminosity value. However, there are a few reasons to have this value as large as possible:

- Large momentum spread helps in the suppression of fast (in comparison with the synchrotron oscillation period) coherent instabilities;
- Increase of the momentum spread leads to increase of the IBS growth times that is proportional to the six-dimensional phase volume.

Maximum momentum spread is limited by

1) the ring dynamic aperture;
2) RF voltage amplitude required to match the short bunch at large ion momentum spread;
3) ion revolution frequency spread tolerable for stochastic cooling system.

The effects 2 and 3 are discussed in Chapter 7.

2nd and 3d limitations are connected with the choice of the ring *momentum slippage factor*

$$\eta_\omega = \frac{1}{\gamma^2} - \frac{1}{\gamma_{tr}^2}. \qquad (2.12)$$

Here γ_{tr} is the Lorentz factor corresponding to the ring transition energy. At a fixed ion momentum spread the RF voltage amplitude and the revolution frequency spread are proportional to the slippage factor (see Chapter 7). Correspondingly, the work with a large momentum spread requires decreasing the slippage factor. It means that the collider has to be operated near the transition energy. On the other hand, the slippage factor has to be large enough to avoid large Coulomb shift of the synchrotron tune, the large slippage factor is preferable for stabilization of slow coherent instabilities. Thus, the momentum spread and the slippage factor have to be chosen as a compromise between many contradictory requirements.

In the estimates below we assume that the ring dynamic aperture permits to accept the momentum spread up to $\Delta p/p = 5\cdot 10^{-4} \div 1\cdot 10^{-3}$ and the momentum slippage factor can be adjusted to the value of about $\eta_\omega \approx 0.03$ in the total range of the experiment energy by appropriate *variation of the ring transition energy.*

3. Interim version of the ring lattice

3.1. General scheme and layout

As we said in the Chapter 1 (Section "Collider 2T"), present version of the collider focusing system is based on the well-developed Nuclotron technology of SC magnets with the cold SC coils and iron yoke, the dipole magnetic field is of 2T. Two collider rings of 336 m circumference (4/3 of the Nuclotron circumference) are placed *one upon the other* and the beam superposition/separation is provided in *the vertical plane*. The collider location (Fig. 1.1, 1.2, 3.1) can be fit to the size of the existing building #205.

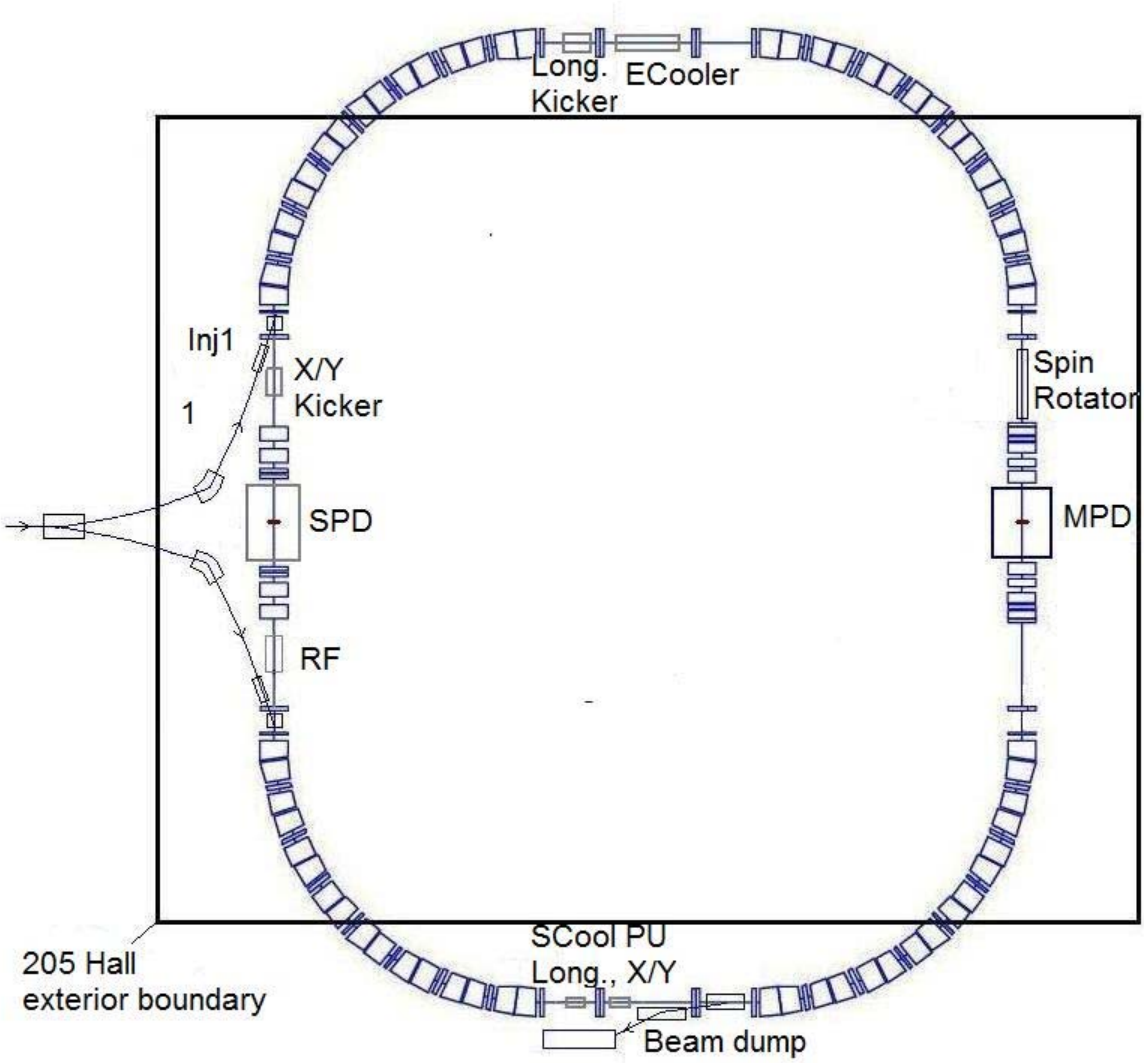

Fig.3.1. Schematic view of the collider ring situated in the building #205

The lattice of the ring consists of 4 bending arcs connected with the 2 long and 2 short straight sections. The correction of the betatron tunes and suppression of the horizontal dispersion functions are produced in the bending arcs. For this purpose the quadrupole lens families are used. The short straight sections are matched to the magnetic structure and used for the location of the experimental devices.

The ring general parameters (Table 3.1) and structural functions (Fig. 3.2, 3.3) have been calculated for certain betatron tune values and for 2 interaction points (IP).

Table 3.1. Main parameters of the collider rings

Ring circumference, m	336
Number of interaction points (IP)	2
Bρ max, T·m	45.0
Ion kinetic energy ($^{197}Au^{79+}$), GeV/u	1.0 ÷ 4.58
Dipole field (max), T	2
Quad gradient (max), T/m	30
Long straight sections: number / length, m	2 / 48
Short straight sections: number / length, m	2 / 24
Free space at IP (for MPD detector), m	9
Beam crossing angle at IP	0
Number of dipoles (arc)/ length, m	64 / 2.2
Number of quads (arc)/ length, m	32 / 0.4
βx_max / βy_max in arc, m	20 / 20
Dx_max / Dy_max in arc, m	6.1 / 0.1
βx_min / βy_min in IP, m	0.5 / 0.5
Dx / Dy in IP1, m	0.0 / 0.2
Betatron tunes Qx / Qy	6.6 / 7.6
Chromaticity Q′x / Q′y	-23 / -26
Transition energy, γ_tr	4.89
Vacuum, pTorr	100 ÷ 10

3.2. Magnetic arc

Each arc consists of the 4 cells of FBDB type. Arc of 48 m length and average radius of 30 m contains 4 focusing and defocusing lenses (F, D) and 16 dipole magnets. The sector dipole has the 2.2 m effective length and 22 m bending radius. The maximum dipole field is about 2 T. 0.4 m long quadrupole has the gradient of up to 30÷35 T/m. The arc lattice allows varying the betatron tune in some range of ±0.5, to suppress the dispersion function in long straight sections (Fig. 3.3).

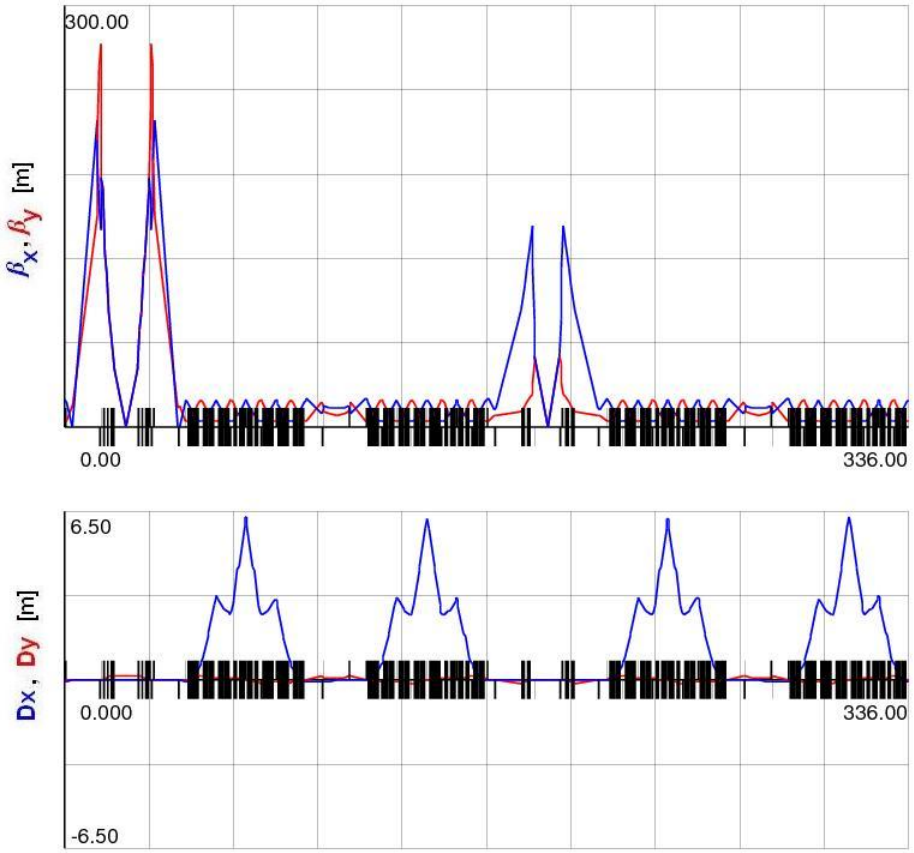

Fig. 3.2. Collider ring: betatron and dispersion functions.

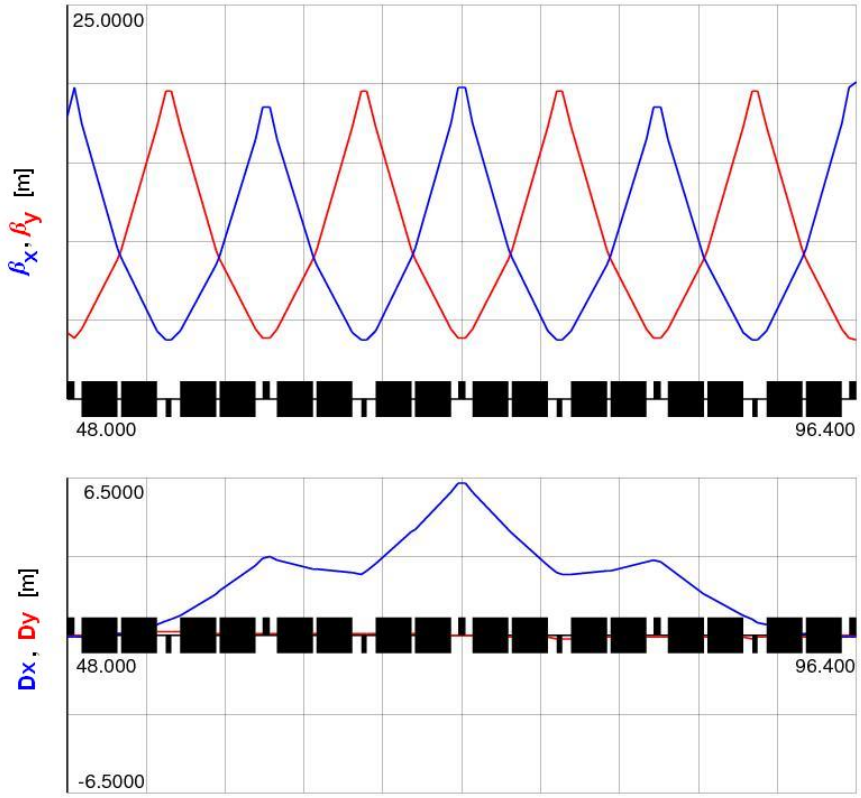

Fig. 3.3. Collider ring: betatron and dispersion functions in arc

3.3. Long straight section 1, interaction point 1 (MPD)

One of 48 m long straight section is used for the arrangement the head-on collision of the circulated beams MPD interaction point. In Fig. 4 the scheme of beam focusing and separation is shown. The location of the separation dipoles and dipole corrector next to the IP allows carrying out the experiments with the different kinds of colliding particle (e. g. Au, p). SC vertical dipoles (1.35 m length, up to 1.5 T max field) provide 0.3 ÷ 0.4 m of 2 ring separation. The 1 m corrector in between makes the additional bend for lower rigid beam. The requirements on beam sizes in IP are met by means (for instance) of quadrupole triplets with the maximum gradient of 60 ÷ 70 T/m.

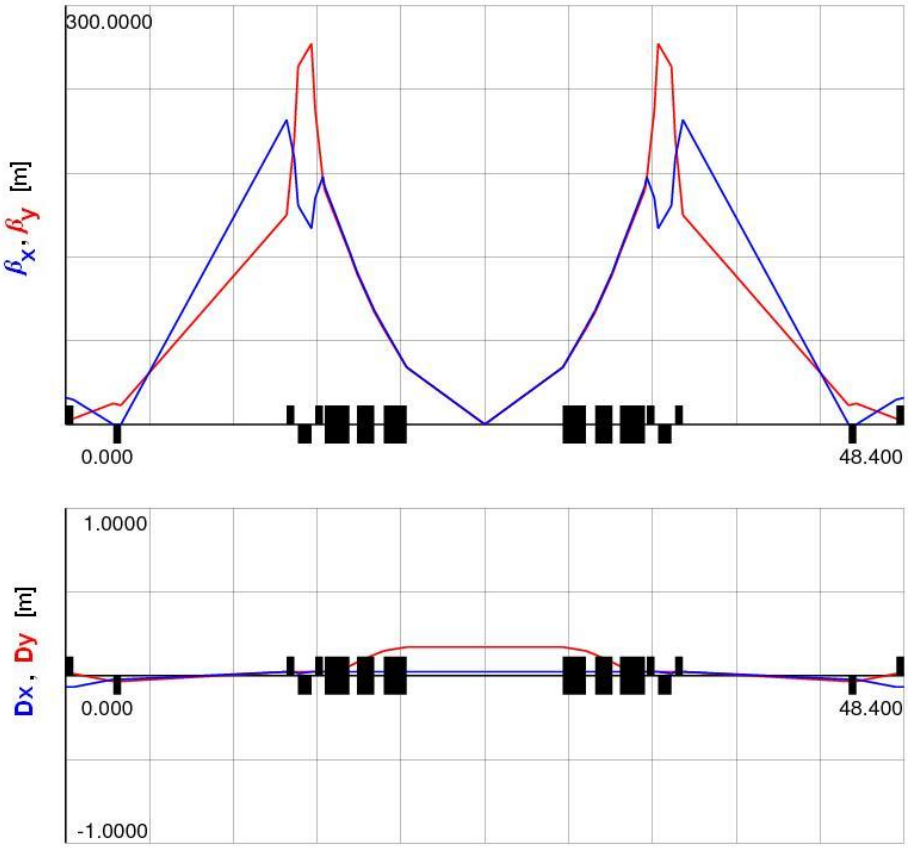

Fig. 3.4. Betatron and dispersion functions in long straight section 1.

3.4. Long straight section 2, the interaction point 2 (SPD).

The requirements for the IP-2 have not been formulated yet. Nevertheless the possibility of insertion of SPD has been included into the collider structure. The head-on collision of polarized protons or deuterons is produced by vertical separation dipoles (1.5 m length, 1.8 T) and quadrupole doublets placed symmetrically around IP-2. In Fig. 5 the amplitude and dispersion functions in 2nd long straight section for the $\beta^* = \beta x = \beta y = 0.5$m are pictured.

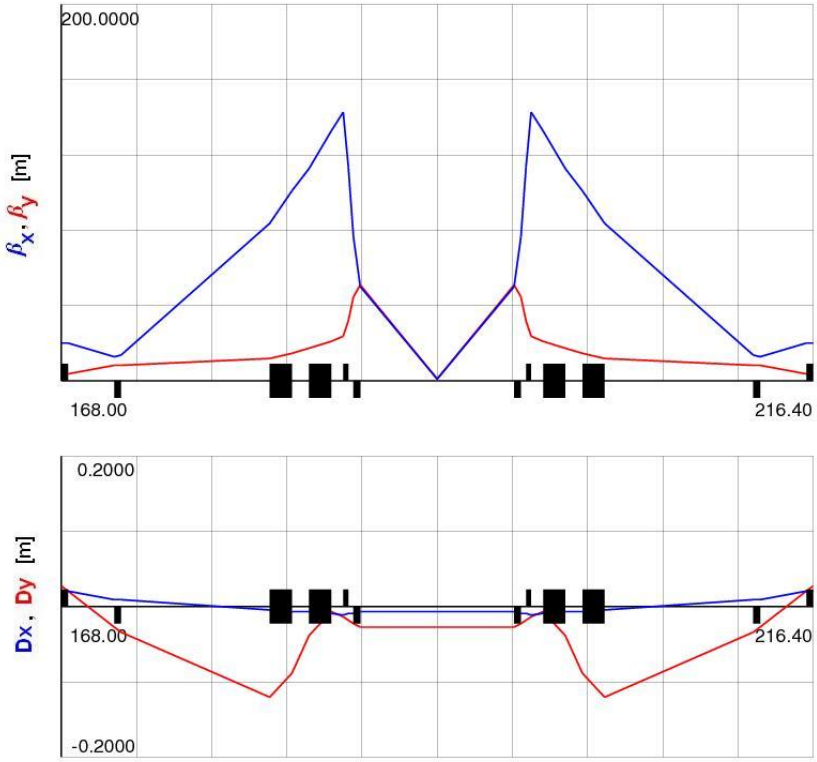

Fig 3.5. Betatron and dispersion functions in long straight section 2 (SPD)

3.5. Short straight section matching

There are 2 short straight sections of 24 m length in each ring. They could be matched to the magnetic arcs providing more space for insertion devices and equipment (Fig. 3.6).

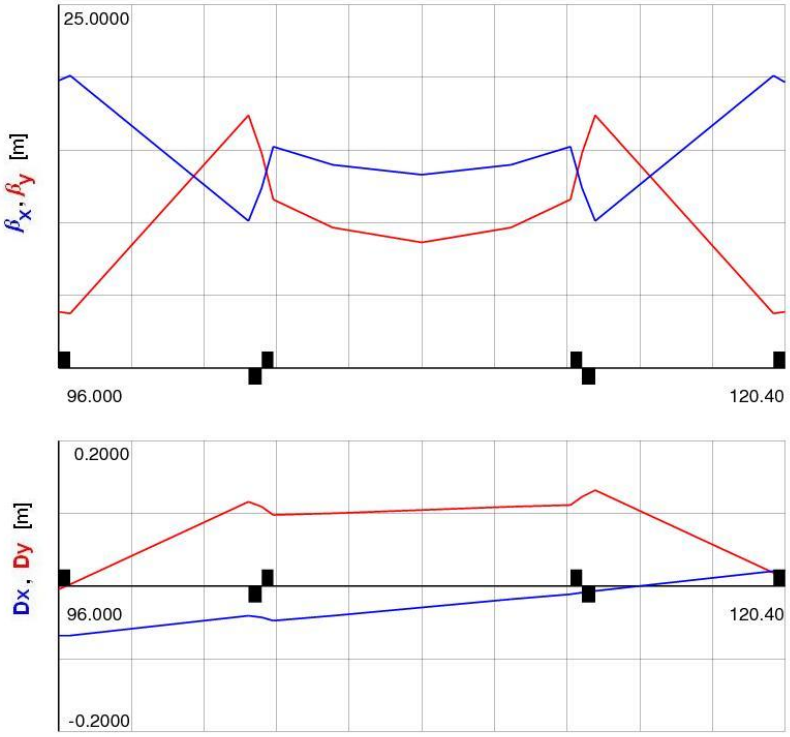

Fig. 3.6. Betatron and dispersion functions in short straight section

3.6. Optics structure in the vicinity of the interaction point

The collider has to provide collisions of mass asymmetric beams including proton-ion (pA) collisions. Alongside of proper physics meaning, it is quite important as a reference point for comparison with heavy ion data. The experiment will be performed at the same MPD detector (Fig.1.3). Therefore the luminosity significantly larger than 10^{27} $cm^{-2}{\cdot}s^{-1}$ is not necessary. This level is achievable quite easily because of large proton number in the beam comparing with heavy ions.

In this mode the collider injection chain has to be switched fast (during a time of a few seconds) from acceleration of heavy ions to acceleration of protons. The heavy ion acceleration is provided by the new heavy ion linac and Booster and after the stripping – by the Nuclotron up to the experiment energy. For the proton acceleration the Booster is not necessary. The proton beam generated by duoplasmatron source is accelerated by LU-20 to 20 MeV of the energy. Single-turn injection permits to have in the Nuclotron more than 10^{11} protons. After adiabatic bunching they are accelerated at the 5-th harmonic of the revolution frequency to the experiment energy and are transferred, bunch by bunch, to the collider ring. If necessary the accelerated proton beam can be rebunched in the Nuclotron after the acceleration to form a single bunch of larger intensity.

For the detector operation the better conditions correspond to equal energy per nucleon independently of the ion species. This demand leads to the independent systems of the deflection and focusing for each ring. In the scheme shown in Fig. 3.1 the triplet lenses are placed behind the vertical deflection dipoles. For the less rigid beam (proton for example) the extra dipole (corrector) is required in between separation magnets to compensate the additional orbit bending in the common dipole. For the same β-function in IP ($\beta^* = \beta_x = \beta_y = 0.5$m) an increase of the triplet distance from the IP leads to increase of the maximum β-function in it (and required beam aperture) (see Fig. 3.4). The parameters of the lattice elements calculated for the Au and proton beams at the same kinetic energy per nucleon of 4.5 GeV/u are presented in Table 3.2.

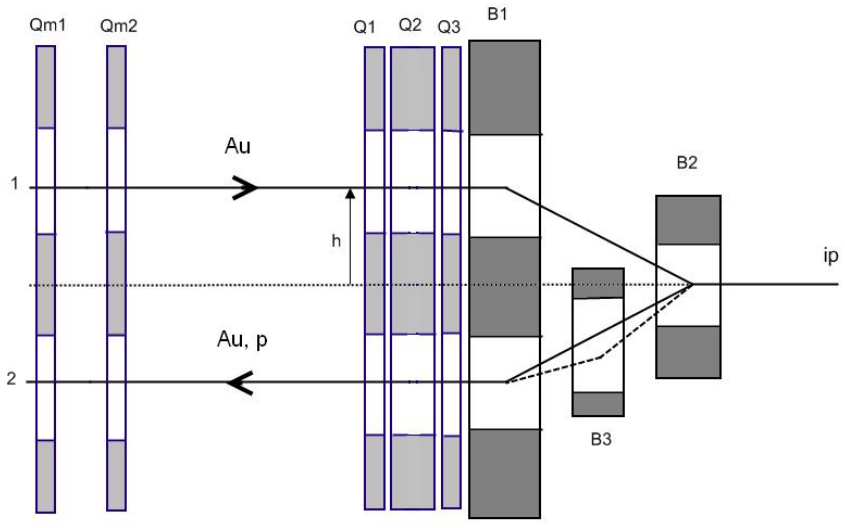

Fig. 3.7. The scheme of the beams separation in the vertical plane for one sort (Au+Au) or different sorts (Au+p) of particles; 2 h = 0.4 m – distance between the median planes of the rings, B – bending magnets, Q – quadrupole lenses.

Such a scheme of the independent beam separation (Fig.3.7) gives a significant flexibility of the collider operation allowing the "symmetric" and "non-symmetric" options of colliding particles. The scheme can be modified in future for non-zero crossing angle (special case not considered here). In such a mode both rings should have independent power supplies for their magnetic systems. The possible design of the quadrupole lenses of large aperture and large field gradient is under preliminary design.

The field value of the bending magnets in beams separation section does not exceed 2 T and quadrupole gradients are relatively low. This permits to use the same technology as for the ring structural magnets and lenses (based on usage of the iron yoke).

Table 3.2. Parameters of the separation system magnetic elements for Au^{+79}: E_k=4.5 GeV/u, Bρ= 44.6 Tm ; p: E_k=4.5 GeV, Bρ= 17.8 Tm.

		Au		p	
	L[m]	K_1 [1/m^2]	G[T/m], B[T]	K_1 [1/m^2]	G[T/m], B[T]
Qm1	0.4	1.19	53	1.19	21
Qm2	0.4	1.47	65	1.47	26
Q1	0.4	1.34	60	1.34	24
Q2	0.8	1.14	51	1.14	20
Q3	0.4	1.04	46	1.04	19
B1	1.35		2		0.8
B2	1.35		2		2
B3	1		-		1.62

3.7. Ring lattice and IBS

The intrabeam scattering (IBS), as written above, is an important effect limiting the collider luminosity. For suppression of IBS we plan to apply stochastic (Chapter 6) and electron (Chapters 9) cooling. However, the task can be simplified very much by proper choice of the ring lattice, because IBS rate decreases significantly if lattice functions are rather smooth. Test of a lattice for this effect we do with the simulations using the code BETACOOL [3.1] and the code developed at Fermilab [3.2]. Both codes were verified in electron cooling experiments and both give closely coinciding results (but differ from MAD by factor of 2 or more).

For instance, the Fermilab code application to the ion beam with parameters listed in Table 2.1 and lattice described in this Chapter gives the IBS growth time values

$$\tau_x = 23 \text{ s}, \ \tau_y = 57 \text{ s}, \ \tau_s = 24 \text{ s}.$$

Correspondingly, BETACOOL code gives

$$\tau_x = 18 \text{ s}, \ \tau_y = 29 \text{ s}, \ \tau_s = 95 \text{ s}.$$

The discrepancy of results obtained with two different codes has likely a trivial explanation: the simulation with BETACOOL has been done using not sufficiently small integration step of the lattice functions over the ring circumference. The reason is of technical character and the problem will be resolved in nearest time. Nevertheless, both results give IBS growth time of the same order and show that the state of the ion bunch formed in the presented lattice is far from equilibrium state from IBS point of view. That is the task for the next step of the ring lattice development.

References

3.1. *http://lepta.jinr.ru*

3.2. S.Nagaitsev, Private communication, 2009

4. Review of beam stability problems

The main space charge effects limiting the beam intensity in the NICA collider are considered in this Chapter. All the numerical estimates have been based on the parameters listed in the Table 4.1.

Table 4.1. Collider beam parameters and luminosity

Energy, GeV/u	1.0	3.5
Ring circumference, m	336	
Betatron tunes	6.6	7.6
Transition energy (GeV)*)	2.3	8.0
Slippage factor η_ω *)	0.030	0.033
Ion number per bunch	5e9	1e9
Number of bunches per ring	32	32
Rms unnormalized beam emittance ε_{un}, π·mm·mrad	5.0	0.34
Rms momentum spread σ_p	1e-3	
Rms bunch length σ_s, m	0.3	0.3
Number of bunches	32	32
Number of RF harmonics	160	160

*) See Chapter 7.

4.1. Bunched beam tune shifts

Betatron tune shifts

Incoherent shift of betatron tunes for bunched beam can be written in the following form (see [4.1], Eq. (4.44)):

$$\Delta Q_{incoh}^{x,y} = -\frac{Z^2}{A}\frac{r_N N_b}{2\pi\beta^2\gamma\varepsilon}\left[\left(\frac{F_b}{\gamma^2}+\beta^2\right)\cdot\left(\frac{a_y}{h}\right)^2\cdot\chi_1^{x,y}+\Phi\beta^2\chi_2^{x,y}\left(\frac{a_y}{g}\right)^2+\frac{F_{SC}\cdot F_b}{2\gamma^2}\cdot\chi_{SC}^{x,y}\right]. \quad (4.1)$$

Here Ze and A are the charge and atomic numbers of the ion correspondingly, r_N is the nucleon classical radius, N_b is ion number perbunch, β and γ are the relativistic factors, F_b is bunching factor (2.6), F_{sc} is image force correction factor (usually $F_{sc} \sim 1$), $a_{x,y}$ are r.m.s. bunch transverse sizes, $2h$ is vertical vacuum chamber size, $2g$ is the gap between dipole magnet poles, $\chi_1^{x,y}$ and $\chi_2^{x,y}$ are so named "Laslett coefficients" [4.2]. Factor Φ is equal to ratio of the orbit length inside dipole magnets to the ring circumference C_{ring}. Coefficient

$$\chi_{SC}^{x,y} = \begin{cases} \dfrac{a_y^2}{a_x\left(a_x+a_y\right)} & \textit{for horizontal oscillations,} \\ \dfrac{a_v}{a_x+a_y} & \textit{for vertical oscillations,} \\ 1/2 & \textit{for round bunch}(a_x=a_y). \end{cases}$$

Factor F_{SC} depends on particle distribution function in phase space. For Kapchinsky-Vladimirsky ("K-V") distribution coefficient $F_{SC} = 1$, for Gaussian beam $F_{SC} = 2$ (and (4.1) coincides with (2.5) at $\chi_{1,2} \to 0$). The exact value of tune shift is calculated by averaging over the machine circumference of $a_{x,y}$, h and g variation.

Coherent tune shift can be written with the following Formula ([1], 4.45)

$$\Delta Q_{coh}^{x,y} = -\frac{Z^2}{A}\frac{r_p N_b}{2\pi\beta^2\gamma\varepsilon}\left[\left(\frac{F_b}{\gamma^2}+\beta^2\right)\cdot\left(\frac{a_y}{h}\right)^2\cdot\xi_1^{x,y}+\Phi\beta^2\xi_2^{x,y}\left(\frac{a_y}{g}\right)^2\right]. \qquad (4.2)$$

Values of all coefficients are given in [1] for set of different vacuum chamber and dipole magnets. For circular vacuum chamber the coefficients are equal to: $\chi_1^{x,y}=0, \xi_1^{x,y}=1/2$. The problem of magnetic coefficients $\chi_2^{x,y}$ and $\xi_2^{x,y}$ is rather complicated and for superconducting NICA magnets it requires a special investigation after the final design. In further estimates we use $\chi_2^{x,y}=\xi_2^{x,y}=0$.

Numerical estimates for parameters from Table 4.1 are presented in Table 4.2 below.

Coulomb shift of synchrotron tune

Space charge shift of synchrotron tune may be found analytically for parabolic dependence of bunch density on longitudinal coordinate ("parabolic bunch"). Electrical field of r.f. system and space charge field of the bunch is defined by

$$E_z = S\left[\frac{qU_0}{2\pi R^2}-\frac{3}{2}\frac{N_b Z_i \chi G_L}{\gamma^2 L_B^3}\right]. \qquad (4.3)$$

In Eq. (4.3) L_B is maximal bunch half-length (in the parabolic bunch r.m.s. half-length $L_b = L_B/\sqrt{5}$), form-factor

$$G_L = 1+2\ln\left(\frac{b}{a}\right).$$

Maximal number of particles per bunch corresponds to zero field; we find

$$N_b^{\max} = \frac{1}{3\pi G_L}\frac{U_0}{U_p}\frac{gL_B^3\gamma^2}{Z_i r_p R^2}. \qquad (4.4)$$

Substituting numbers we have $N_b^{\max} = 2.33\cdot 10^9 \quad (h=160)$. The synchrotron tune $Q_s = \Omega_s/\Omega_0$ is determined as follows:

$$Q_s = Q_s^0\sqrt{1-N_b/N_b^{\max}} \qquad (4.5)$$

where synchrotron tune for zero intensity is defined as following:

$$Q_s^0 = \frac{1}{\beta}\sqrt{2\pi h|\eta_\omega|\cdot\frac{Z}{A}\frac{eU_0}{\gamma m_N c^2}}\text{, where } \eta_\omega = \frac{1}{\gamma^2}-\frac{1}{\gamma_{tr}^2}$$

is slippage factor, γ_{tr} is transition Lorentz factor, m_N – nucleon mass. Ion momentum spread is connected with ion bunch length with the following Formulae:

$$\sigma_p = Q_s\cdot\frac{\sigma_s}{|\eta_\omega|R}. \qquad (4.6)$$

Let us underline that it is necessary to provide the condition

$$\frac{N_b}{N_b^{\max}} << 1.$$

One of reasons: coherent instability of dipole longitudinal oscillations ("*rigid mode*"). To suppress this instability the synchrotron tune shift $\left(\Delta Q_s^{coh} \approx N_b / 2N_b^{\max}\right)$ should be less that incoherent spread of synchrotron tunes (this condition provides necessary Landau damping). The second reason: momentum spread for $N_b = N_b^{\max}$ is equal to zero, that results to microwave instabilities.

4.2. Single bunch coherent instabilities

We have considered five effects:

1) Longitudinal and transverse microwave instabilities (similar to coasting beam ones).
2) Longitudinal and transverse coupling mode instabilities.
3) Weak head –tail (due to the ring chromaticity).

The driving force for the microwave instabilities usually is considered as "broadband resonator" (on cut-off frequency). For the longitudinal and transverse coupling mode instabilities and weak head – tail the driving force is resistive impedance.

Longitudinal mode of the microwave instability one uses usually the well known *Keil-Schnell formula* [4.4] that describes the instability threshold peak current:

$$I_{peak} \le \frac{4\beta^2\gamma A}{Z} \cdot \frac{m_N c^2}{e} \cdot \frac{|\eta_\omega|\sigma_{1/2}^2}{|Z_L / n|} \cdot F_L \ .$$

Here $Z_L/\mathbf{n}$ is the longitudinal coupling impedance Z_L dividing on mode number n, $\sigma_{1/2}$ is half-width on half height (for Gaussian distribution $\sigma_{1/2}$ is about r.m.s. momentum spread). The longitudinal impedance includes impedance of the vacuum chamber and the space-charge impedance

$$\frac{Z_L^{SC}}{n} = \frac{Z_0 G_L}{2\beta\gamma^2} \ , \ G_L = 1 + 2\ln\left(\frac{b}{a}\right)$$

$Z_0 = 377\ Ohm$ ($Z_0 \cdot c \approx 12.3$) is the longitudinal form factor, a and b are the beam and vacuum chamber radii correspondingly, Ze is the ion charge; β, γ are the relativistic factors, $m_N c^2$ is the nucleon rest energy, A is the ion atomic number, η_ω is the ring *momentum slippage factor*:

$$\eta_\omega = \frac{1}{\gamma^2} - \frac{1}{\gamma_{tr}^2} \ . \qquad (4.7)$$

The parameter γ_{tr} is Lorentz factor corresponding to transition energy. Factor $F_L = 1$ for the standard Keil-Schnell criterion. Let us underline that K-S criterion with $F_L = 1$ is sufficient one (in fact it corresponds to negative mass instability below the critical energy); for necessary criterion factor F_L depends on the distribution function in momentum space and parameter

$$u = \frac{|\mathrm{Re}(Z_L)|}{|\mathrm{Im}(Z_L)|},$$

where R_s is shunt impedance of the broadband cavity. For the most realistic Gaussian distribution and $u << 1$ factor F_L is about 10-20 (by artificial construction of long tail distributions it is possible to increase F_L up to 100-200 [4.5]).

The peak current is connected with ion number per bunch N_{bunch} by the formula

$$I_{peak} = \frac{ZeN_{bunch}}{T_{rev}} \frac{C_{Ring}}{\sqrt{2\pi}\sigma_s}$$

Then Keil-Schnell formula can be rewritten for numerical estimates here in a simplified form:

$$N_{KS} \le 1.6 \cdot \frac{\beta^2 \gamma^3 A}{Z^2 r_N} \cdot \frac{\sigma_s \sigma_p^2 |\eta_\omega| \cdot F_L}{1 + 2 \cdot ln(b/a)} \qquad (4.8)$$

Numerical estimates results presented below in the Table 4.2 show that an attempt to keep ΔQ_{incoh} = const in all the energy range leads to a *large discrepancy at ion energy of 1 GeV/u* with Keil-Schnell criterion if we use "the reference parameters values". It means that one needs to conduct much more accurate analysis and choice of collider parameters. This task we postpone until Chapter 12.

Table 4.2. Bunch parameters limitations

Ion energy, GeV/u	1.0	3.5
Ion number per bunch	5e9	1e9
Rms unnormalized beam emittance ε_{un}, π·mm·mrad	25.0	0.34
Rms momentum spread σ_p	1e-3	
Rms bunch length σ_s, m	0.3	
ΔQ_{incoh}	–0.054	
ΔQ_{coh}	–0.011	–1.6e-4
$(N_{bunch})_{KS}$	0.28	4.6

Substituting Z_L^{sc} and expressing σ_p through I_{Peak} we obtain:

$$\sigma_p^{tr} = \sqrt{\frac{Z_0 I_{Peak}\left[1 + 2 ln\left(\frac{a}{b}\right)\right]\chi Ze}{4 F_L A m c^2 \beta^3 \gamma^3 \left|\frac{1}{\gamma^2} - \frac{1}{\gamma_{tr}^2}\right|}}. \qquad (4.9)$$

We will consider two approaches: 1) "pessimistic" scenario (F_L = 1); 2) "optimistic" scenario ($F_L(u)$ is calculated for Gaussian distribution and $u = R_s/(Z_L)^{SC} << 1$). The calculated dependence of σ_p and σ_p^{tr} on kinetic energy E are given in Fig. 1, 2 for R_s /n= 1 *Ohm*; it was assumed that the beam emittance has linear dependence on E; $\gamma_{tr} = 4.95$.

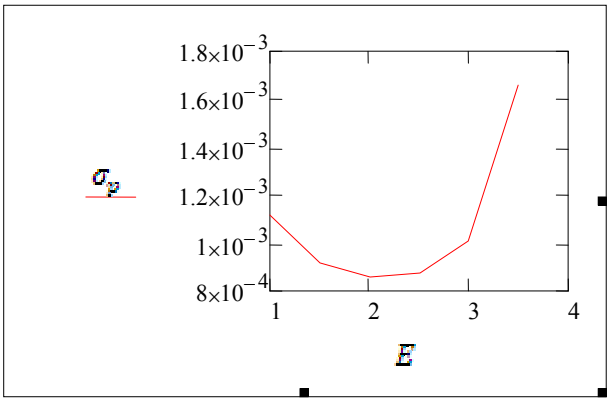

Fig. 4.1. Dependence of σ_p on kinetic energy

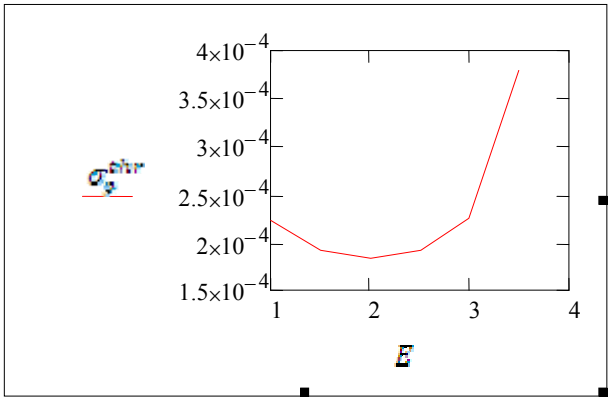

Fig. 4.2. Dependence of σ_p^{tr} on kinetic energy for $F_L =$ (values are varied in range 20–25).

Transverse microwave instability

Microwave transverse instabilities (similar to transverse instability of unbunched beam) can appear in bunch if the following conditions are valid:

1) wavelength of the perturbation is much less than the bunch longitudinal length;

2) the instability growth rate is much larger than the synchrotron tune $\left(Im\left(\Delta Q_c\right) = Im(a)/\Omega_0\right)$.

This growth rate is equal to

$$\mathrm{Im}\left(\Delta Q_c\right) = \frac{Z_i}{A_i}\frac{I \cdot R}{2\pi Q\beta\gamma}\mathrm{Re}\left(Z_\perp\right). \qquad (4.10)$$

This instability is suppressed by Landau damping. For coasting beam the stability criterion (Keil-Zotter criterion [4.6]) can be written as follows:

$$I \le 4F_t \frac{mc^2}{\chi|Z_\perp|R}\frac{A_i}{Z_i}\beta\gamma Q\,. \qquad (4.11)$$

Here $(\Delta Q_n)^{1/2}$ is effective spread on betatron tunes for mode with number n (half-width on half height), F_t is form-factor depending on distribution function on transverse invariants and transverse impedance (as sufficient condition we can use $F_t = 1$). It is defined by

$$\Delta Q_n \approx \sqrt{\left[(n-Q)\eta+\xi\right]^2\left(\Delta p_{1/2}\right)^2 + \left(\Delta Q_{non}\right)^2}\,. \qquad (4.12)$$

In Eq. (4.12) ξ is the ring chromaticity, ΔQ_{non} is the non-linear tune spread due to external non-linearity, $\Delta p_{1/2}$ is momentum spread (half-width on half height). To apply this criterion to the bunched beam we should replace current in Eq. (4.10) on the maximal current in the bunch [4.7] (it is possible since the instability has local character). For Gaussian beam

$$I_{\max} = \frac{ZeN_b\beta c}{\sqrt{2\pi}L_b}\,.$$

Due to short bunch length (0.3 m) the most appropriate candidate as "driving force" is broadband cavity. Then the instability appears at cut-off frequency $\omega_c = c/b$; corresponding mode number $n_c = \omega_c/\Omega_0 = R/\beta b$. For cut-off frequency $Re(Z_\perp) = (R_\perp)^s$, where $(R_\perp)^s$ is transverse shunt impedance of broadband cavity. Due to high value of n_c we can neglect the contributions from chromaticity and the nonlinearity. Then we obtain that $\Delta Q_n \approx n_{cut}\cdot|\eta_\omega|\cdot(\Delta p/p)$. Substituting this expression in Eq. (4.12) and rewriting it relative σ_p we come to the following result:

$$\sigma_p^{tr} = \frac{1}{4F_t}\frac{I|Z_\perp|R}{U_p}\frac{1}{\beta\gamma Q n_{cut}|\eta|}\,. \qquad (4.13)$$

Here $Z_\perp = iZ_\perp^{sc} + R_s^\perp$, where space charge impedance

$$Z_\perp^{sc} = \frac{Z_0 R}{\beta^2\gamma^2}\left(\frac{1}{a^2} - \frac{1}{b^2}\right). \qquad (4.14)$$

and $(R_\perp)^s$ is transverse shunt impedance of broadband cavity ($(Z_\perp)^{SC} >> (R_\perp)^s$). For $F_t = 1$ we find that $(\sigma_p)^{tr} = 5.953$. This value considerably exceeds designed value of the momentum spread ($\sigma_p \sim 10^{-3}$). Strictly speaking we should use values of F_t corresponding to the stability diagram; then for Gaussian distribution and $u = (R_\perp)^s / ((Z_\perp)^{SC} << 1$ corresponding values of F_t are about 3-4.

Let us underline that dispersion relation derived in paper [4.6] is not correct in presence of r space charge non-linearity; in this case it is necessary to use correct dispersion equation, derived in paper [4.8]. Analysis of this dispersion is made at the last paper Burov and Lebedev [4.9]. According this paper the threshold momentum spread is defined by

$$\sigma_p = \frac{1}{n_{cut}|\eta|}\frac{|\Delta Q_{sc}(0)|}{1.7\cdot\ln\left(\frac{|\Delta Q_{sc}(0)|}{\mathrm{Im}(\Delta Q_c)}\right)}. \qquad (4.15)$$

In this equation $\Delta Q_{sc}(0)$ is maximal incoherent shift of the betatron tune at the bunch center, which for bunch with Gaussian longitudinal and transverse distributions and axial symmetry ($\varepsilon_x = \varepsilon_y$, $Q_x = Q_y$) is defined as follows:

$$\Delta Q_{sc}(0) = \frac{N_b r_i}{\pi\beta^2\gamma^3\varepsilon_x}\frac{L_C}{\sqrt{2\pi}\sigma_s}\cdot \mathrm{Im}(\Delta Q_c)$$

is defined by Eq. (4.4). Let us mark that Eq. (4.8) is valid only if $\Delta Q_{sc}^x(0) >> \mathrm{Im}(\Delta Q_c)$. It is easy to see that

$$\frac{|\Delta Q_{sc}(0)|}{\mathrm{Im}(\Delta Q_c)} = \frac{Z_\perp^{sc}}{R_s^\perp}.$$

Calculated dependence $(\sigma_p)^{tr}$ on energy is built at Fig. 4.3.

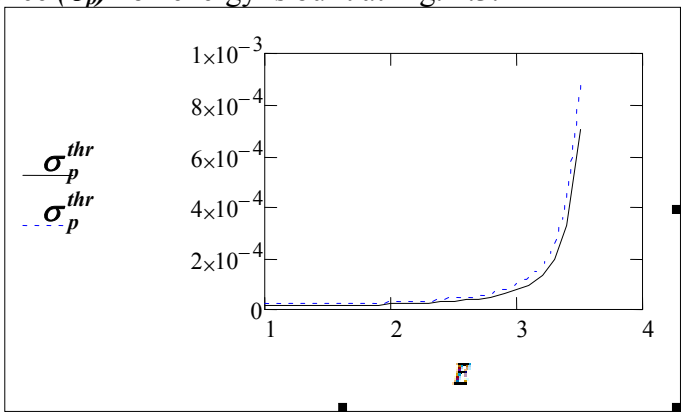

Fig.4.3. Dependence of threshold momentum spread σ_p^{thr} on energy E (GeV/n).
Solid curve corresponds to $(R_\perp)^s$ = 0.2 MOhm/m, corresponds to $(R_\perp)^s$ = 1 MOhm/m.

We see that threshold value of σ_p is less than 10^{-3} in all energy range.

Transverse coupling mode instability (*strong head-tail*)
The simplest method of modeling strong head-tail effect is use of two-particle model [4.10]. This model for a case of constant wake with amplitude W_0 shows that the beam stability depends on parameter

$$\Upsilon_{\perp}^{tr} = \frac{\pi r_0 N_b W_0 c^2}{4\gamma L_C Q_{\perp} Q_s (\Omega_0)^2}. \qquad (4.16)$$

Fast and crucial instability appears if $\Upsilon_{\perp}^{tr} \geq 2$. In a frame of two-particles model a reason of this instability is coupling of "sum" mode of oscillations ($\boldsymbol{u = (y_1 + y_2)/2}$, where $\boldsymbol{y_{1,2}}$ are transverse coordinates of two-particles) and "difference" mode ($\boldsymbol{\upsilon = (y_1 - y_2)/2}$. Condition $\Upsilon_{\perp}^{tr} = 2$ allows us to find limitation for wake amplitude

$$\boldsymbol{W_0 \leq W_0^{thr} = \frac{8\gamma L_C Q_{\perp} Q_s (\Omega_0)^2}{\pi r_0 N_b c^2}}. \qquad (4.17)$$

Substituting numbers for NICA we find that $\boldsymbol{W_0^{thr} = 18\ cm^{-2}}$ (in SGS units). Corresponding transverse impedance in Ohm/m is

$$\boldsymbol{\tilde{Z}_{\perp}^{th} = \frac{bZ_0}{4\pi} W_0^{lim}}.$$

For NICA $\boldsymbol{\tilde{Z}_{\perp}^{th} = 1.89 \cdot 10^5}$ Ohm/m; this limitation is strict enough. Let us mark that two-particle model is very rough and usually underestimate the effect.

More correct way is application of Sacherer integral equation derived by use of perturbation theory [4.11]. For small intensity modes of perturbation theory (proportional to $\boldsymbol{\exp(im\theta_s + il\theta_y)}$, where $\boldsymbol{\theta_s}$ is longitudinal phase, $\boldsymbol{\theta_y}$ is transverse one) are isolated; dispersion equation transforms in a set of separated equations for modes with different ***m,l***. With intensity increase the equations become coupled. This coupling can be analyzed only by use of numerical methods; results depend on depends on chosen stationary distribution on variable $\boldsymbol{I_s}$ (longitudinal action) and the impedance characteristics. A.W. Chao is studied the mode coupling ([4.5], Eq.6.5) for broad-band impedance

$$\boldsymbol{Z_0^{\parallel}(\omega) = R_0 \left|\frac{\omega_0}{\omega}\right|^{1/2} |1 + i \cdot \mathrm{sgn}(\omega)|}, \qquad (4.18)$$

where $\boldsymbol{R_0}$ is real positive constant. This impedance corresponds to diffraction model with wake $\boldsymbol{W_0^{\parallel}(z) \propto |z|^{-1/2}}$. Numerical estimates using the Chao's analytical formulae have shown that the limitation, corresponding to two-particle model, is softened in 2–3 times.

Let us underline that $\boldsymbol{Q_s \sim \sqrt{|\eta|}}$ and therefore this instability becomes more dangerous if we approach to transition energy.

Longitudinal coupling mode instability

In analysis given in Chao's textbook it is used "water-bag" distribution, which results to degeneration of the radial modes of perturbation theory. The analysis has shown that the bunch stability depends on dimensionless parameter

$$\boldsymbol{Y_{\parallel} = \frac{N_b r_0 \eta R_0}{\gamma \omega_s^2} \left(\frac{c}{T_0 L_b}\right)^{3/2}}. \qquad (4.19)$$

The threshold value of this parameter $\boldsymbol{Y_{\parallel}^{th} - 1.45}$; if $\boldsymbol{Y_{\parallel} > Y_{\parallel}^{th}}$ the fast instability appears. Analysis of Chao results has shown that for NICA parameters the transverse coupling mode instability have more high growth rate than the longitudinal one. However longitudinal instability can be more dangerous since it is suppressed only the Landau damping caused by non-linearity of synchrotron oscillations, which is very small for small synchrotron tune.

Weak head-tail instability.

According to A. Chao ([4.5], p. 201) the growth rate of weak "head-tail" instability (derived by two-particles model) is defined by the following formula:

$$\frac{1}{\tau_+} = \mp \frac{r_i N_b W_0 \xi_n L_b}{2\pi\gamma L_C \eta}. \qquad (4.20)$$

In this equation the normalized chromaticity $\xi_n = \xi / Q$, W_0 is an amplitude of transverse wake in cm^{-2}, which is assumed to be constant. Normalized increment (in betatron tune units)

$$\Delta Q_{ht} = \mp \frac{r_i N_b W_0 \xi_n L_b}{2\pi\gamma L_C \eta \omega_0(E)}. \qquad (4.21)$$

Let us mark that sign "+" is related to sum mode (oscillations of the center of gravity), sign "–" corresponds to the difference mode. When the sum mode is unstable, the difference mode is stable (and vice versa). Thus below the transition energy ($\eta > 0$) and natural sign of chromaticity ($\xi < 0$) the sum mode is damped and the difference mode is anti-damped. However two particles model underestimates an increment of the difference mode and for small increments high order modes can be stable due to Landau damping. These considerations are forced to choose small negative values of ξ below the transition energy.

However to make it we should have the chromaticity correction circuit!

Of course, two particle model underestimates the effect. In Ng's lectures [Eq. (12-1)] weak head-tail is analyzed by use of Sacherer dispersion equation for water-bag distribution. Increment of mode with number m is defined by (Eq.12.2):

$$\frac{1}{\tau_m} = -\frac{1}{1+m}\frac{Z_i}{A_i}\frac{\chi c I_b}{4\pi E_0 \omega_\beta}\int_0^\infty \mathrm{Re}\left[Z_\perp(\omega)\right]\left[h_m(\omega-\omega_\xi) - h_m(\omega-\omega_\xi)\right]d\omega. \qquad (4.22)$$

Here $\omega_\xi = \xi\omega_0/\eta$ is the betatron tune shift because of chromaticity ξ, $\omega_\beta = Q\omega_0$, and function $h_m(\omega)$ is energetic spectrum of mode with number m. From this formula we see that instability is absent is $\xi = 0$. Let us consider resistive impedance, which is defined by (Ng, Eq. (1.44)):

$$Z_\perp(\omega) = \left[1 - i\,\mathrm{sgn}(\omega)\right]\frac{cL}{\pi\omega b^3 \sigma_c \delta_{skin}}. \qquad (4.23)$$

Here σ_c is the chamber conductivity, δ_{skin} is skin layer depth. Analysis of this equation for NICA parameters has shown that the mode with number $m = 2$ is the most dangerous one. Its increment is defined by:

$$\frac{1}{\tau_z} = 0.095\frac{1}{3}\frac{Z_i}{A_i}\frac{\chi c I_b}{4Q\gamma E_p}\sqrt{\frac{2}{\omega_0\tau_L}}\left|Z_\perp(\omega_0)\right|. \qquad (4.24)$$

This instability is suppressed by Landau damping, which appears because of synchrotron tune spread or non-linear spread on betatron tunes. Numerical analysis that for NICA parameters spread on synchrotron tunes does not suppress the instability. For its damping it is necessary to use chromaticity correction circuit or octupole circuit creating non-linear spread on betatron tunes (however this circuit can diminish the dynamical aperture [4.12]).

Let us underline that both considered models does not take into account influence of space charge forces, which stabilizes weak head-tail according the last studies [4.13]. However this problem needs in further investigation. We believe that the most prospective method is numerical modeling with application of real wake-functions. Spectacular example of such approach is given in [4.12], where is studied influence of kickers on particle dynamics in SPS. In measurements process it was discovered that 40% of the transverse coupling impedance in SPS is connected due to kicker-magnets with ferrite. This work includes the following main parts: 1)

results on dipolar and quadrupolar kicker impedance from Tsutsui's theory); 2) CST simulations and theory); 3) HEADTAIL dynamics simulations with updated impedance models.

Multi-bunch instabilities.
The main reasons of multi-bunch instabilities in NICA are high order modes (HOM) in accelerating cavities and resistive impedance of the chamber. However due to the small amount of bunches ($\boldsymbol{q = 20}$) the growth rates of these instabilities are not so large. We should mark that half of chamber is cold that diminishes the resistive impedance. As concerns HOM usually shunt impedances and quality factors in the ion machines are not very high due to variation of r.f. frequency. Nevertheless it is necessary to be careful and suppress dangerous HOM.

Conclusions
Chosen beam parameters for NICA seems to be realizable with using of the following cures:

- Suppression of high order modes (HOM) in accelerating cavities.
- Design of good chamber with small coupling impedances (shunt impedances of broad-band resonator: $R_s^{\parallel}/n \sim 1-2$ Ohm, $\boldsymbol{R_s^{\perp} \sim 0.2-0.8}$ MOhm/m).
- Use of the chromaticity correction circuit for suppression of high order head tail modes (or octupole families to increase non-linear Landau damping).

References

4.1. K. Y. Ng, *Physics of Intensity Dependent Beam Instabilities*, Fermilab-FN-0713, Long Beach, CA, 2002.
4.2. L.J. Laslett, Proc. Of 1963 summer Study on Storage Rings, BNL-Report 7534, p.324; L.J. Laslett and L. Resegotti, Proc. of VI Int. Conf. on High Energy Accelerators, Cambridge, MA, p.150, 1967.
4.3. A.W.Chao, *Physics of Collective Beam Instabilities in High Energy Accelerators*, John Wiley and sons, 1993.
4.4. E. Keil, W. Schnell, *Concerning longitudinal stability in the ISR* CERN-ISR-TH-RF-69-48 ; ISR-TH-RF-69-48, 1969.

4. 5. D.G. Koshkarev and P.R. Zenkevich, *Stabilization of Longitudinal Instabilities in Heavy Ion Storage Rings*, PTE, v. 4, p. 3, 1982.

4.6. B. Zotter and F. Sacherer, CAS CERN 77-13, p.175, Geneva, (1977).

4.7. D. Boussard, CERN Lab II/RF/Int 75-2 (1975); R. D. Ruth and J. M. Wang, IEEE Transactions on Nucl. Sci. NS-28, p.2405 (1981). This is called Boussard criterion in the literature.
4.8. D. Mohl and H. Schonauer, Landau damping in non-linear space-charge forces and quadrupoles, Proc. Of IX Int. Conf. on High Energy Accelerators, Stanford, p.380, 1974; see also D. Mohl, Report No. CERN/PS 95-08 (DI), 1995.
4.9. A. Burov and V. Lebedev, *Transverse instabilities of coasting beams with space charge*, PRST-ACCELERATORS AND BEAMS **12**, 034201, 2009.
4.10. C. Pellegrini, Nuovo Cimento **64**, p.447, 1969; M. Sands, SLAC-TM-69-8.
4.11. F. G. Sacherer, *Theoretical Aspects of the Behavior of Beams in Accelerators and Storage Rings*, Proc. First Course of Int. School on Part. Accel., Erice, Nov. 10-22, p.198, 1976.
4.12. V. Kapin, V. Kornilov, „Simulations of octupole induced effect on dynamic aperture in SIS-100", https://www.gsi.de/documents/ACC-note-2009-06.html.
4.13. M. Blaskiewicz, *Fast head-tail instability with space charge*, Phys. Rev. ST Accel. Beams **5**,044201, 1998; A. Burov, *Head-tail Modes for Strong Space Charge*, Phys. Rev. ST Accel. Beams **12**,044202-1, 2009; V. Balbekov, FEMILAB-PUB-09-322-APC, 2009;V. Kornilov and O.Boine-Frenkenheim, *Simulation Studies@Code Validation for the Head-*

Tail Instability with Space Charge, Proceedings of ICAP2009, San Francisco, 2009.
4.14. E. Métral, G. Rumolo, B. Salvant, C. Zannini, *Update on the impedance of the SPS kickers*, SPS impedance meeting, Oct. 16th 2009.

5. Beam stacking with barrier buckets technique, stochastic cooling of coasting beam

5.1. Working cycle of the collider operation

To provide independent optimization of the bunch intensity, bunch number and to control the beam emittance and momentum spread during the bunch formation we plan ion storage in the collider of a *coasting beam initially*.

Such a scheme simplifies significantly the requirements to the injection chain. The beam storage is planned to be realized in longitudinal phase plane with application of RF barrier bucket technique. Under a cooling the number of the injection pulse can be large enough without decrease of the stacking efficiency. In the case the intensity of the injected portion influences on the stacking process duration only and can be arbitrary in principle. The required beam emittance is formed during the stacking by the *cooling application*.

The NICA collider injection chain is designed for acceleration of about 10^9 ions at the repetition rate of about one pulse during 5 s. Store $(3\div6)\cdot10^{10}$ ions in each ring will require of about 10 minutes. Even at the injection intensity of one order less the storage time will be sufficiently shorter than the experiment duration, therefore the mean luminosity will be close to the peak one.

A barrier RF system is a broad-band RF system comprising of ferrite loaded RF cavities with RF wave forms generated using solid state wide-band power supplies. One can also generate some specific wave forms using fast switches. The storage can be performed using movable or fixed burrier voltage pulses. After storage of a required ion number the barrier voltage is switched off. After the beam began to be coasting it can be bunched at harmonics number equal to the bunch number required at collisions. The bunching can be realized by feeding the same broad band cavity with sinusoidal RF of the required frequency. After the bunching completion the bunch compression will be performed by the RF phase jump, and the short bunch will be matched with RF at higher harmonics providing by another cavity.

At this scheme the collider has to be equipped with the broad band cavity of the Barrier Bucket RF system and the cavity operated during collisions at large harmonics number that is necessary to keep a short bunch length at reasonable RF voltage.

If the IBS heating is suppressed by a cooling the luminosity decreases during the experiment due to particle loss in single scattering with residual gas atoms and recombination in the electron cooling section. The particle loss can be compensated from time to time by addition of new ions using the same storage scheme. For this the high harmonics RF is switched off and the storage is provided using barrier bucket system.

5.2. Beam stacking at fixed Barrier Bucket and stochastic cooling

During the beam stacking the stochastic cooling application is more preferable than the electron one because it does not lead to additional particle loss. The required cooling rate is sufficiently less than that one during collision experiment because small peak beam current. At a barrier RF bucket application the particle density inside the bucket is almost uniform. Therefore the IBS

growth rates increase in comparison with a coasting beam by a factor equal to ratio of the ring circumference to the bucket length only.

The parameters of both barrier RF bucket ans stochastic cooling systems are rather modest (Table 5.1).

Table 5.1 Stochastic Cooling & Barrier Voltage Parameters

Ion beam	
Ions	$^{197}Au^{79+}$
Beam kinetic energy, GeV/u	3.5
Number of ions per inection shot	1e8
Initial r.m.s. momentum spread $\sigma_{initial}$ (truncated at +/-3 $\sigma_{initial}$)	3.0e-4
Transverse emittance, π·mm·mrad,	0.3 (constant)
Ring slippage factor / Transition Gamma	0.0232 / 9.16
Stochastic cooling system	
Cooling method	"Palmer"
Slippage factor from PU to Kicker	0.0232
Type of Pickup and Kicker	λ/4 loop coupler
Atmospheric Temperature at PU, K	300
Noise Temperature at PU, K	40
TOF from PU to Kicker, μs	0.4
Dispersion at PU and Kicker, m	5.0 and 0
Number of PU and Kickers	128
Loop length / height / width, mm	24.5 / 50 / 50
Coupling impedance, Ohm	50
Band width, GHz	2-4
Gain, dB	90
Barrier voltage system	
Barrier voltage, kV	$\pm$ 5
Barrier frequency, MHz / Period, μs	5.0 / 0.2
Injection kicker pulse width, nsec	400

The separatrix height $\Delta p/p$ for the barrier voltage 5kV is 1.4e-3 (Fig.5.1). When the particle momentum exceeds this separatrix height, the particle is no more trapped in the stable region.

To estimate achievable efficiency of the stacking process the numerical simulations were performed [5.1]. Simplest storage scheme utilizes fixed barriers. Such a scheme with electron cooling was experimentally tested at ESR in GSI [5.2].

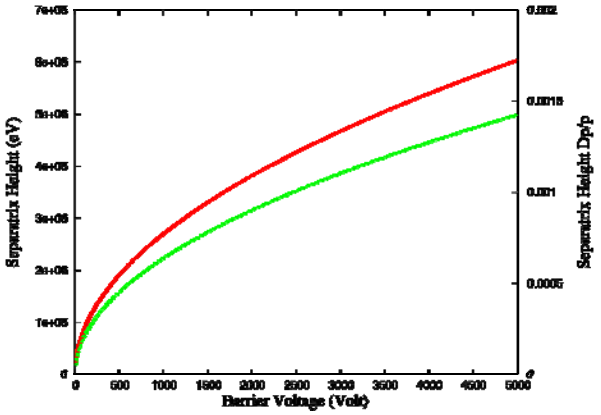

Figure 5.1 Separatrix height, energy ΔE (red, left scale) and momentum spread $\Delta p/p$ (green, right scale) vs barrier voltage.

The voltage applied to the RF gap consists of two pulses that divide the longitudinal phase plane by two regions – with stable and unstable phase motion. The injection is provided into the unstable region (Fig. 5.2a). Due to the cooling almost all the particles are concentrated inside the stable region (Fig. 5.2b) after that the new injection can be performed.

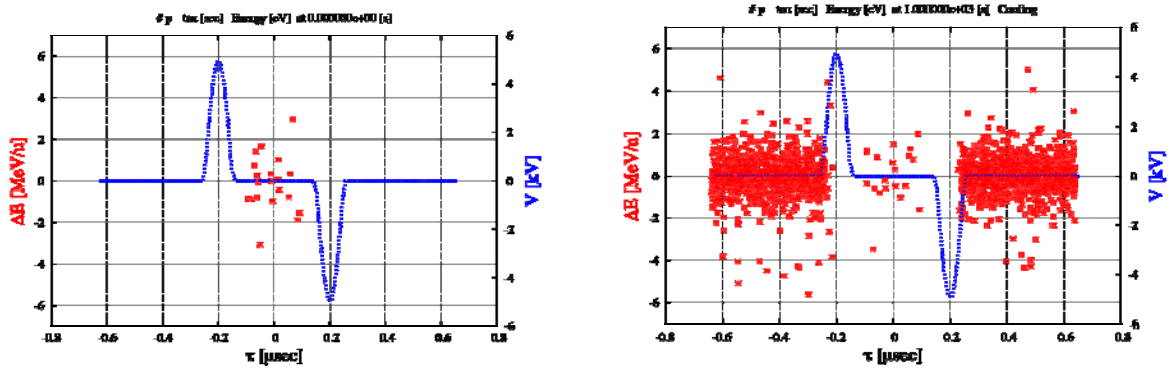

a) b)

Fig. 5.2 The illustration of principle of beam accumulation with fixed barrier bucket: the red points are particles in the phase space, the left scales in both Figures 5.2 are particle energy difference from the synchronous energy 3.5 GeV/u, the horizontal scale is time, one revolution period; the blue lines in both Figures are barrier voltages (right scale); Fig.5.2a shows the illustartion after the 1st batch injected, the Fig.5.2b shows the case after 100 batches injection.

The stacking efficiency depends on the particle loss during a new injection: the particles located in the unstable region will be killed by an injection kicker pulse. The efficiency can be optimized by appropriate choice of the injection intensity and repetition time and the cooling power (Fig.5.3).

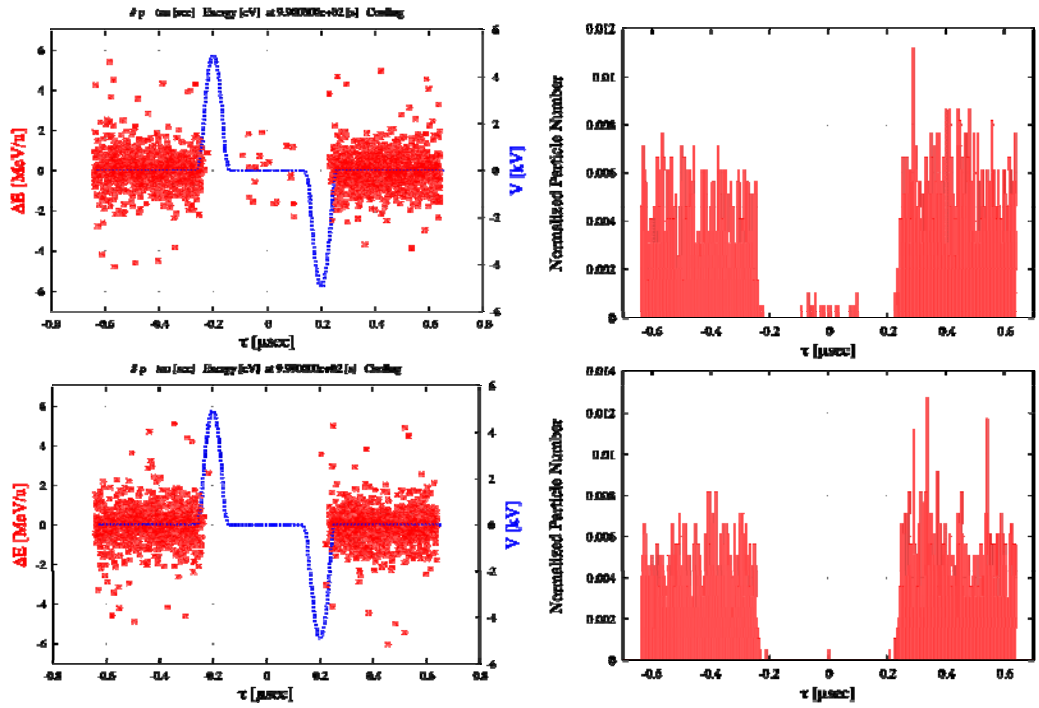

Figure 5.3 Particle distribution in phase space after 99th batch injected, time=990.0 sec (top left) and particle distribution along the ring (top right). After 9 sec later, time=999.0 sec, (bottom left and bottom right).

The simulations performed for gold nucleus at 3.5 GeV/u of the kinetic energy and at the *collider circumference of 366 m* showed that the storage efficiency during as minimum 100 injection pulses can be achieved at the level not less than 95%. The simulations were performed for the bunch parameters expected at extraction from the Nuclotron: $\sigma_p = 3 \cdot 10^{-4}$ at the bunch duration of about 200 ns. The injection intensity was chosen of 10^8 ions that expected at the first stage of the collider operation.

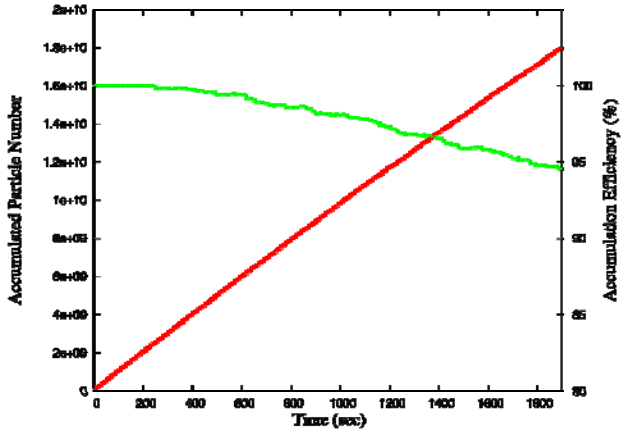

Figure 5.4 Accumulated particle number (red) and accumulation efficiency (green) during the stacking process up to 190th stacking.

The bandwidth of the stochastic cooling system was chosen to be of 2 GHz (from 2 to 4 GHz), the required amplifier power does not exceed 100 W. Even at such moderated parameters the stochastic cooling system provides the cooling rate large enough to form small momentum spread of the stack required for further beam bunching (Fig. 5.5).

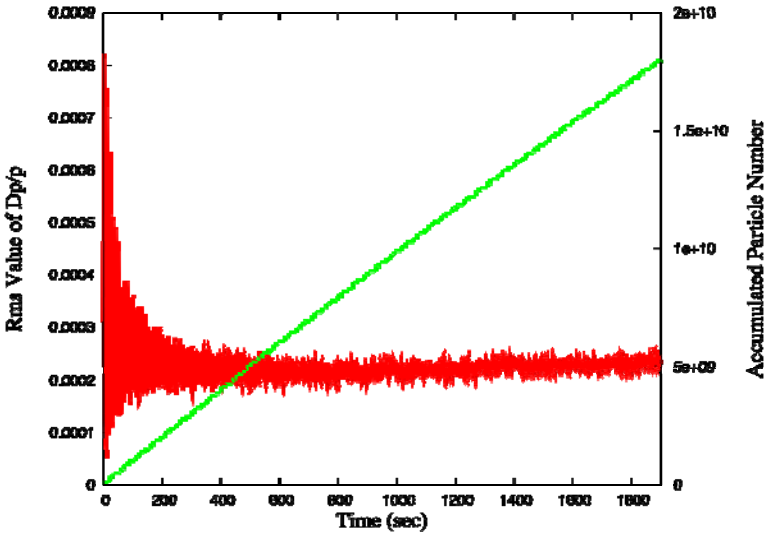

Fig. 5.5. Evolution of the beam momentum spread and
stacked particle number during the stacking process up to 190th stacking.

Summary of the simulation results

1. We assume the injection particle number from Nuclotron= 1e8/shot. With use of barrier voltages of +/- 5000 Volt, and stochastic cooling system, we can accumulate the 3.5 GeV/u 197Au79+ ions in the NICA collider up to 200 times and we will obtain 2e10 ions in the collider ring. Injection cycle is 10 sec which is fit to the Nuclotron operation cycle. Then we need 2000 sec to get the above numbers of beam in two collider rings. That is short enough period for the beam accumulation.

2. The advantage of present injection scheme are as follows
1) The pulse length of injected beam from the Nuclotron is assumed as 0.2e-6 sec, around the 1/3 of the Nuclotron ring circumference. Then we do not need the bunch rotation system in the Nuclotron ring.
2) The rms momentum spread assumed in the present simulation is as large as 3e-4 (rms value) which could be attained without the electron cooling at the booster ring.
3) The momentum spread of stacked coasting beam of 2e10 ions, is small enough as corresponding $\Delta p/p$ is around 2.0e-4. Then the electron cooling system is not necessary in the collider rings.

3. After de-bunching the stacked beam, we will apply the RF of ~200 kV and 20 MHz frequency (just 20 times of revolution frequency in the collider) to the de-bunched coasting beam adiabatically and apply the stochastic cooling. Finally we obtain the 20 bunches, each containing 1e9 ions. Each bunch length is around 0.3 m (rms). This bunching process is described in the Chapter 6.

5.3. Prototype of the broad band cavity for the NICA collider

The voltage amplitude required for efficient stacking of the beam depends on the ring momentum slip factor. In the simulations in the previous paragraph the slip factor was about 0.02. In this case the voltage amplitude required to keep the particles inside the stack is 2 kV.

A few barrier bucket systems are in operation in the world (for instance, in 4 rings at FNAL) and the required parameters corresponds to well established area. For instance, as a prototype of the NICA collider broad band cavity can be chosen the cavity designed in FZJ (Juelich) for HESR ring of the FAIR project (Fig. 5.6).

Fig. 5.6. The broad band cavity designed in FZJ for HESR.

The cavity consists of two tanks with a total length of about 80 cm including the acceleration gap. The maximum voltage at the gap is 5 kV at cw mode of the operation. Upper designed frequency for this cavity is 5 MHz that is not enough for the NICA storage scheme, however the cavity impedance in the high frequency region is about 200 Ohm and weakly depends on the frequency.

The outer diameter of this cavity is slightly less than 60 cm that is compatible practically with the NICA collider design where the distance between the ring median planes is between 30 and 40 cm.

The cavity designed in BINP (Novosibirsk) for RF system of the NICA Booster [5.5] has similar parameters, except the geometry dimensions determined by chosen ferrite rings. It seems to reasonable to design and construct the collider broad band cavities in cooperation with BINP also.

References

5.1. T. Katayama, Stochastic cooling at NICA project, Interim report, October 2009, Dubna.
5.2. C. Dimopoulou, et. al., Experimental demonstration of longitudinal ion beam accumulation with electron cooling, Proc. of EPAC08, Genoa, Italy.

5.3. C. M. Bhat, Barrier RF systems in synchrotrons, Proceedings of EPAC 2004, Lucerne, Switzerland. References 5.3, 5.4 are not quoted!
5.4. R. Stassen et. al., The HESR RF-system and tests in COSY, Proc. of EPAC08, Genoa, Italy.
5.5. V.Arbuzov et al., Report on research work dedicated to development of the concept of the RF acceleration station for NICA Booster, Budker INP, Novosibirsk, 2008.

6. Bunched beam formation and stochastic cooling

6.1. Bunched beam formation

After ion storage with barrier bucket technique application (Chapter 5) the coasting and stochastically cooled ion beam has to be bunched. This procedure is performed by three stages:
1) Adiabatic capture with harmonic RF in the buckets of 32nd harmonics (at stochastic cooling ON, if necessary – the option to be considered),
2) Bunch rotation in longitudinal phase space with RF phase "jump",
3) Bunch capture in high frequency bucket with formation by such a method sufficiently short bunch.

Numerical simulations have been performed for the following parameters:

$$E_{ion} = 3.5 \text{ GeV/u}, \; C_{Ring} = 336 \text{ m}, \; \eta = 0.02.$$

Stage 1: Adiabatic capture with harmonic RF in the buckets of 32nd harmonics. V_{RF} adiabatically varies from 50 V to 10 kV during 0.5 s, initial $\sigma_p = 3 \cdot 10^{-5}$, final $\sigma_p = 3 \cdot 10^{-4}$, $\sigma_s = 0.56$ m.
Stage 2: Bunch rotation in longitudinal phase space with RF phase "jump" (3 steps).
Stage 3: Capture into 160th harmonics, $V_{RF} = 50$ kV.
Final bunch parameters:

$$\sigma_p = 3.65 \cdot 10^{-4}, \; \sigma_s = 0.28 \text{ m}.$$

In the following section we will see that stochastic cooling "alone" allows reaching of necessary σ_p and σ_s values without bunch interception in high RF harmonics.

6.2 Stochastic cooling of the bunched beam in collision mode

The stochastic cooling process of bunched beam was simulated by T.Katayama for the *Palmer method* using the code developed during 2007-2009 in collaboration with NICA group. The simulation was done for parameters close to those of present version of the NICA collider ("Version 2T"). Some parameters listed in Table 6.1 differ from those of used above. However, this difference is not critical for the present consideration.

One of the important results obtained by T.Katayama is demonstration of possible application of *the same stochastic cooling system* both to stacking process and to cooling of the bunched beam in collision mode.

In the simulation longitudinal ion motion is analyzed, i.e. bunch *transverse emittance is kept constant*. Development of both three-dimensional simulation and accounting the space charge repulsion force is the task for further studies.

IBS process in the ion bunch is taken into account as a competing one with the stochastic cooling. IBS growth rate of ion momentum spread is calculated with Martini formulae and the result can be fitted with the following equation:

$$Growth\ Rate = 10^{-9.20} \cdot (\Delta p / p)^{-2.30} \qquad (6.1)$$

Table 6.1. Parameter list for stochastic cooling simulation

Ring circumference, m	375
Ion beam parameters	
Ions	$^{197}Au^{79+}$
Ion energy, GeV/u	3.5
Number of ions: per bunch	1e9
Initial r.m.s. momentum spread σ_p	1.5e-3
Initial bunch length σ_s, m	18.75 (64 nsec)
Ion longitudinal distribution in bunch	uniform
Transverse emittance, π·mm·mrad	0.3 (constant)
RF system and related parameters	
Ring slippage factor η_ω	0.0232
RF Voltage, kV	100, 200, 400
Harmonics number	20
Stochastic cooling system and related parameters (Palmer stochastic cooling method)	
Number of PUs and kickers	128
Dispersion at PU, m	5.0
Dispersion at kicker, m	0.0
Time of flight from PU to kicker, μs	0.4
Band width, GHz	2 ÷ 4
Pickup Impedance, Ohm	50
Gain, dB	90
Microwave power, W	100
Atmospheric Temperature, K	300
Noise Temperature, K	40

In the present simulation, IBS heating term is calculated at every computing cycle with use of this fitting equation.

The goal of the simulation is to find the equilibrium condition parameters: the equilibrium values of ion momentum spread σ_p (rms), bunch length l_s (rms) and the RF voltage amplitude V_{calc}. The last one is calculated with small amplitude synchrotron oscillation formula for attained σ_p and σ_s values. The equilibrium condition is the balance of beam cooling, RF field and the heating mechanism, mainly by IBS heating. An essential parameter is the time of equilibrium state attainment $\tau_{equi.}$

Below we present characteristic graphs for cooling process for the case of the attainment of the optimal (project) equilibrium beam parameters (Fig. 6.4 ÷ 6.8).

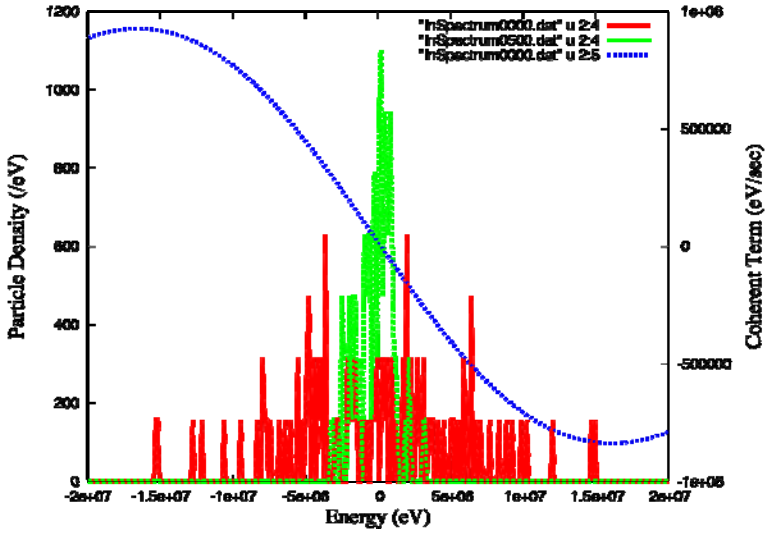

Fig.6.4. Coherent term (eV/s) of stochastic cooling system (blue)- right scale:
ion distribution (eV^{-1}) over energy before (red) and after (green) 100 sec cooling- left scale;
the horizontal scale is ion energy.

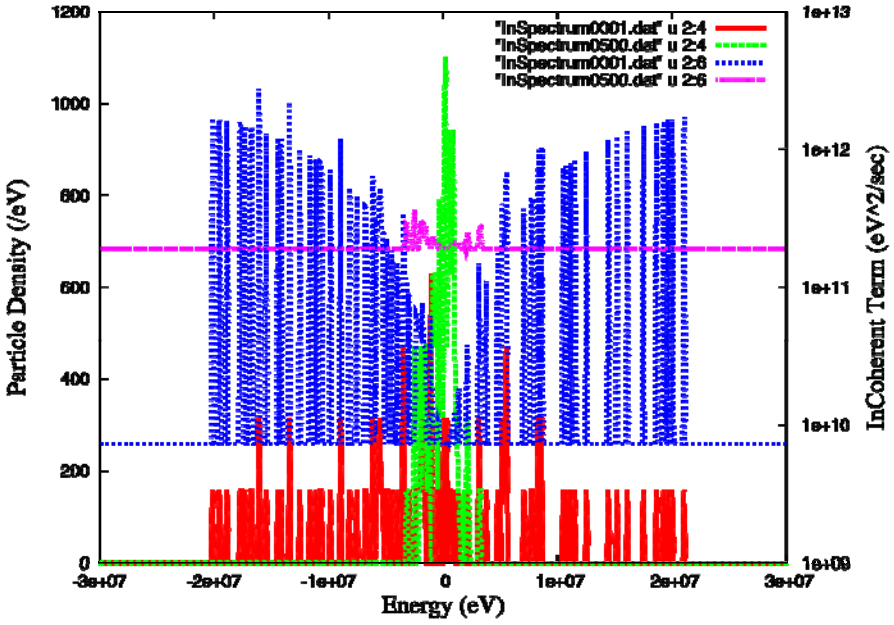

Fig.6.5. Incoherent term (eV^2/s) before (blue) and after (pink) 100 sec. cooling
and ion distribution (eV^{-1}) over energy before (red) and after (green) cooling.

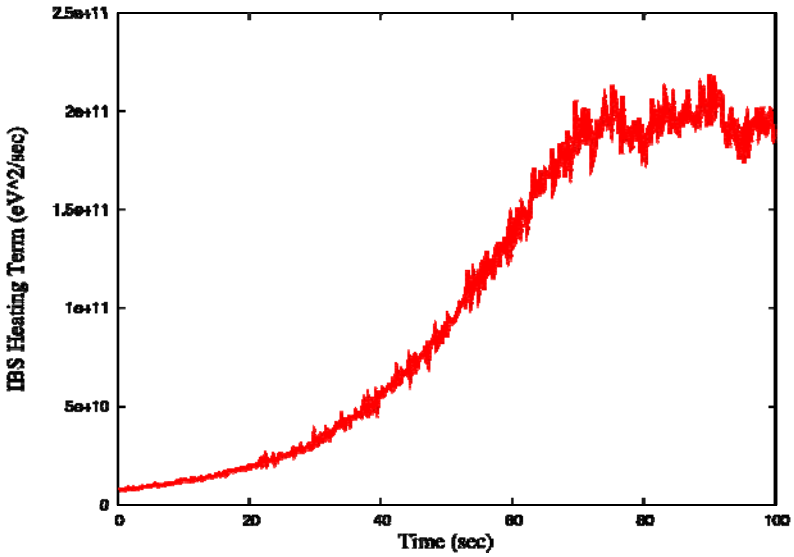

Fig.6.6. IBS heating term (eV^2/s) during cooling process

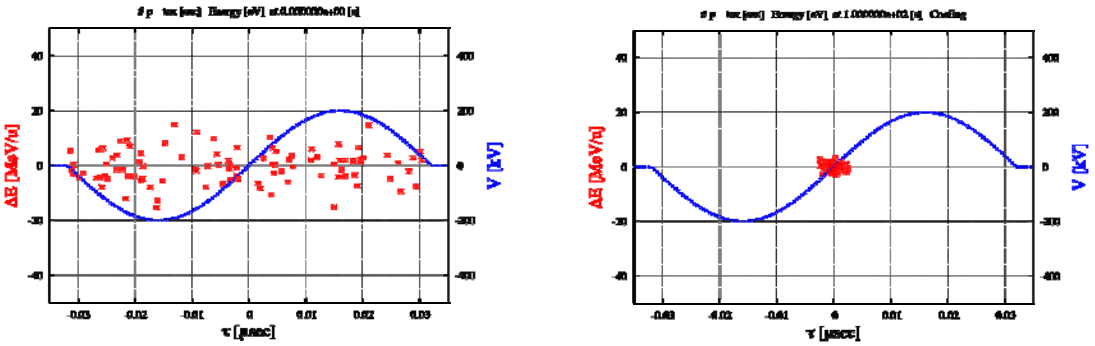

a) b)

Figure 6.7 Ion distribution in the longitudinal phase space (ΔE, τ): before cooling (a) and after 100 sec cooling (b); the RF voltage is 200kV (blue curve).

The presented graphs do demonstrate an effective cooling of ion bunch of project parameters with equilibrium attainment for 100 sec. Comparison of the simulation results (Table 6.2) one can conclude that bunch project parameters can be reached in 100 sec after beginning of the cooling process.

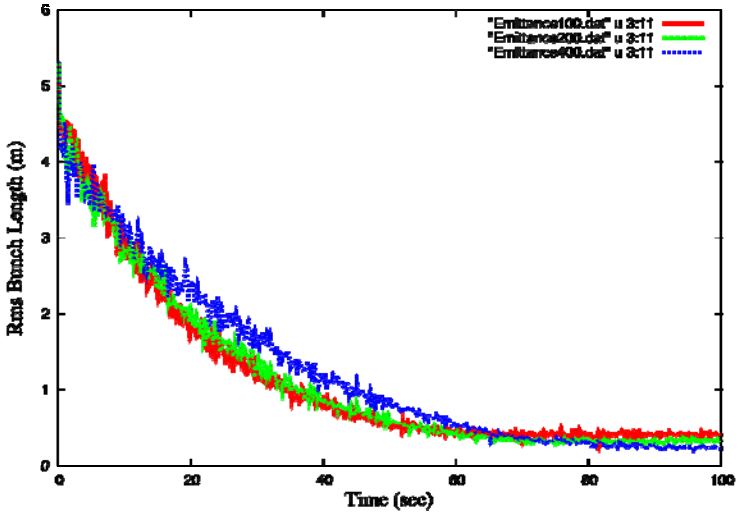

Figure 6. 8 Evolution of rms bunch length (m) during the cooling process for different RF voltage. 100kV(red), 200kV(green) and 400kV(blue).

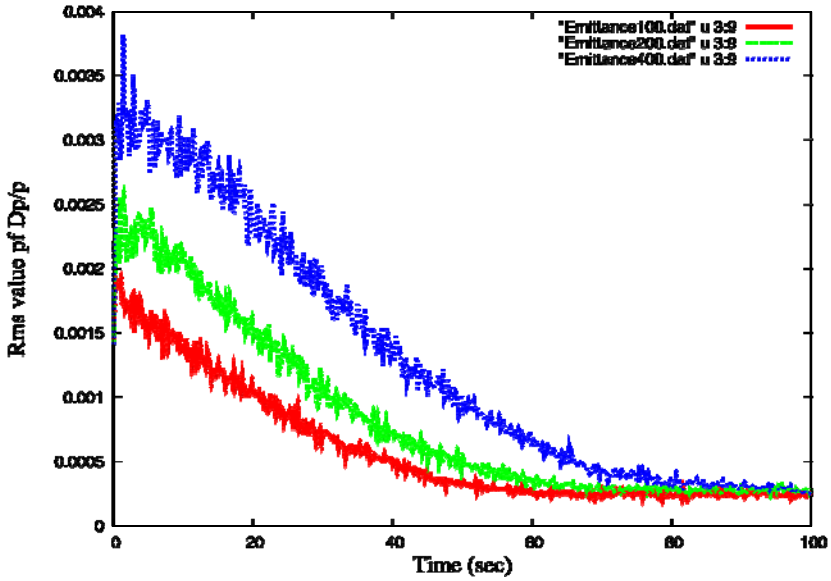

Figure 6.9 Evolution of rms value of Dp/p during the cooling process for different RF voltage. 100kV(red), 200kV(green) and 400kV(blue).

Table 6.2. Results of stochastic cooling simulation

RF voltage [kV]	τ_{equi} [s]	σ_p [1e-4]	σ_s [m]	V_{calc} [kV]
100	~ 60	2.4	0.408	95.2
200	~ 70	2.83	0.322	212
400	~ 100	2.65	0.225	381

One should note that bunch interception into high harmonics (h ~ 200) allows reduction of the RF voltage amplitude (see next Chapter).

7. RF system parameters and requirements on critical energy tuning

Parameters of the Collider RF system are defined by several very different effects. The most critical of them are the following

1) Criteria defined by stochastic cooling application,
2) Collider beam stability,
3) Restrictions of technical character.

7.1. Criteria defined by stochastic cooling application

An efficient operation of the stochastic cooling system requires meeting certain conditions for collider parameters. First of them is avoiding of overlapping of revolution frequency harmonics bands. It means that for given ion momentum spread $\sigma_p \equiv \Delta p/p$ the value of the slippage factor η_ω (see definition (2.12) or (4.7)) has to be taken sufficiently small. Indeed, the "gap" between the $(n+1)^{st}$ and n^{th} harmonics is equal to ion revolution frequency f_s and the band width at n^{th} harmonics is described as

$$\delta f_n = n f_s \eta_\omega \sigma \ . \qquad (7.1)$$

The maximum value of harmonics number n_{max} is equal to ratio of the is maximum frequency f_w of the stochastic cooling system *band width* w to ion revolution frequency f_s :

$$n_{max} = f_w / f_s \ .$$

The condition of not overlapping can be written as (Fig.7.1)

$$6 \cdot \delta f_n < f_s \text{ at } n = n_{max} \ , \qquad (7.2)$$

where factor 6 has been added here for Gaussian distribution of ions over momentum.

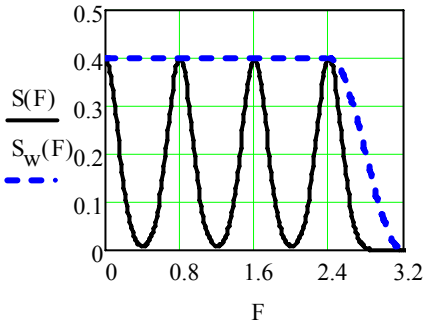

Fig.7.1. An example of feedback system spectrum near the spectrum cut-off (dash curve) and revolution frequency harmonics spectrum (solid curve) at an outmost case of harmonics not overlapping: F= f_w – 3.2 MHz, f_s = 0.8 MHz (C_{Ring} = 366 m, β = 1), $\delta f_n = (n/n_{max})*f_s/6$.

Then one can write the requirements to η_ω value as function of ion energy E_A:

$$\eta_\omega(E_A) < \frac{f_s(E_A)}{6\sigma_p f_w} \ . \qquad (7.3)$$

For the NICA collider parameters (f_s = 0.78 ÷ 0.88 MHz, σ_p = $1 \cdot 10^{-3}$, f_w = 4 GHz) it gives the upper limit of η_ω as ion energy function E_A (Fig.7.2):

$$0.03 < \eta_{max}(E_A) < 0.034 \ . \qquad (7.4)$$

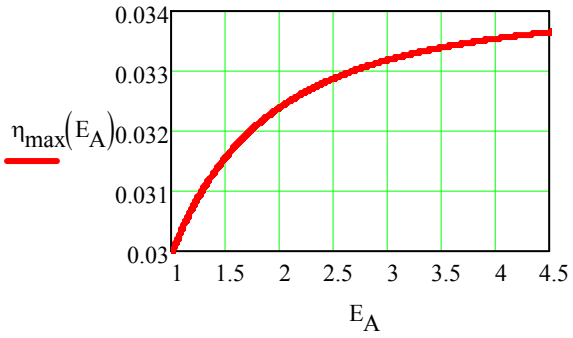

Fig.7.2. Maximum slippage factor vs ion energy
for stochastic cooling system parameters described above the Formula 7.4.

7.2. Collider beam stability. Keil-Schnell criterion

As a first approximation, one can consider in this Chapter *the coherent (microwave) instability* as the main danger and use the criterion for the *longitudinal mode* of the microwave instability - the *Keil-Schnell criterion* [Chapter 4, Formula (4.8)] that describes the instability threshold ion number per bunch N_{KS} by the formula

$$N_{KS} \le 1.6 \cdot \frac{\beta^2 \gamma^3 A}{Z^2 r_N} \cdot \frac{\sigma_s \sigma_p^2 |\eta_\omega| \cdot F_L}{1 + 2 \cdot ln(b/a)} \qquad (7.5)$$

(see symbols explanation in Chapter 4). One should underline also that *the chamber impedance* $Z_{chamber}$ *is not included* in this formula. It has to be taken into account if

$$Z_{chamber} \sim (Z_L)_{SC} \sim \frac{400}{\beta\gamma^2} \; . \qquad (7.6)$$

If $Z_{chamber} << (Z_L)_{SC}$ one can take the factor $F_L = 10$ (see Section 4.2).

The criterion (7.5) allows finding the lower limit of η_ω. Therefore it would be useful to present here the ion bunch number N_{KS} as functions of ion energy at different values of η_ω (Fig. 7.3).

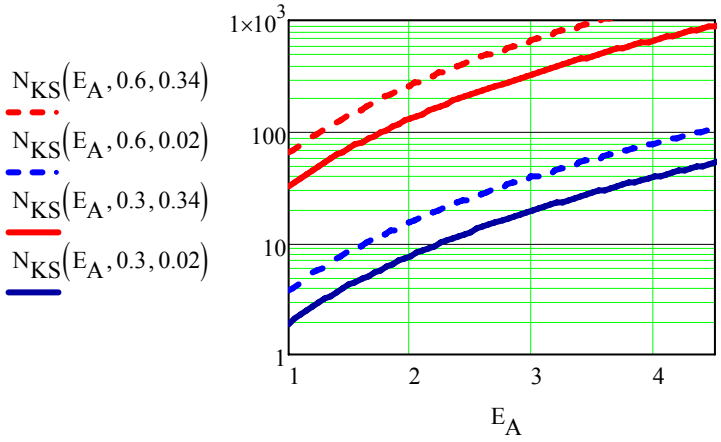

Fig. 7.3. N_{KS} (in units of 10^9) vs ion energy (Keil-Schnell criterion)
for $\eta_\omega = 0.034$ and 0.02, $\sigma_p = 1 \cdot 10^{-3}$, $\sigma_s = 0.6$ (dash curves) and 0.3 (solid curves) m, $F_L = 10$.

One can see that KS-criterion allows to have ion number per bunch above 1e9 in all energy range of the Collider at

$$0.02 < \eta_\omega < 0.034$$

if $\sigma_p = 1 \cdot 10^{-3}$ and $\sigma_s \ge 0.3$ m.

7.3. Limitations of RF system parameters

Our goal when designing RF system is to choose collider parameters in such a way that the RF amplitude does not exceed of 200 kV. For *small oscillation amplitude* of ions inside harmonic RF bucket the RF voltage amplitude, V_{RF}, is given as following:

$$V_{RF} = \frac{|\eta_\omega| \cdot \beta^2 \gamma}{2\pi h} \cdot \frac{A}{Z} \cdot \left(\frac{C_{Ring}}{\sigma_s} \cdot \sigma_p \right)^2 \cdot \frac{m_N c^2}{e}, \qquad (7.7)$$

where h is harmonics number. The V_{RF} value has certain technical restrictions, which in our case of tunable frequency are more severe than for fixed frequency system. One can consider as a more or less realistic value of the upper limit of the RF voltage amplitude

$$V_{RF} \le 200 \text{ kV}. \qquad (7.8)$$

This restriction requires corresponding optimization of bunch parameters. One can see (Fig.7.4) that bunch length $\sigma_s = 0.3$ m at $\sigma_p = 1 \cdot 10^{-3}$ and $\eta_\omega = 0.03$ does not meet the condition (7.8). Due to this reason further we choose

$$\sigma_s = 0.6 \text{ m}. \qquad (7.9)$$

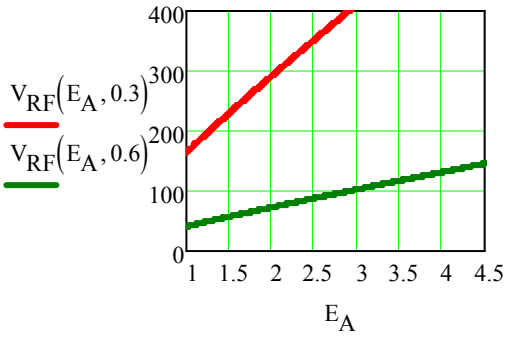

Fig.7.4. V_{RF} vs ion energy at $\sigma_s = 0.3$ and 0.6 m, $\sigma_p = 1 \cdot 10^{-3}$ and $\eta_\omega = 0.03$.

Below (Chapter 12) we will see that the required luminosity level can be achieved at $\sigma_s = 0.6$ m.

7.4. Problems and tasks

Summarizing the consideration done in Sections 4.1 ÷4.3 one can conclude that slippage factor value has to be chosen in the range

$$0.02 < \eta_\omega < \eta_{max}(E_A), \qquad (7.10)$$

where $\eta_{max}(E_A)$ is described by Formula 7.3. It follows from here that with energy variation the ring lattice has to be tuned in such a way that value of transition energy (Lorentz factor γ_{tr}) provides fulfillment of condition (7.10). Correspondingly, minimum value of V_{RF} should be chosen as shown in Fig. 7.5a, b.

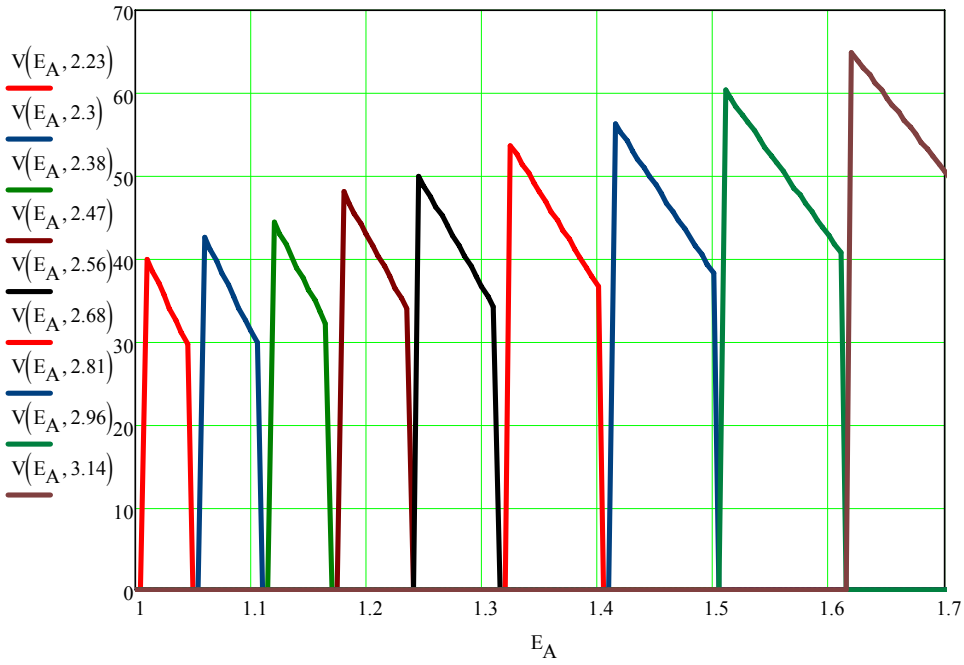

a)

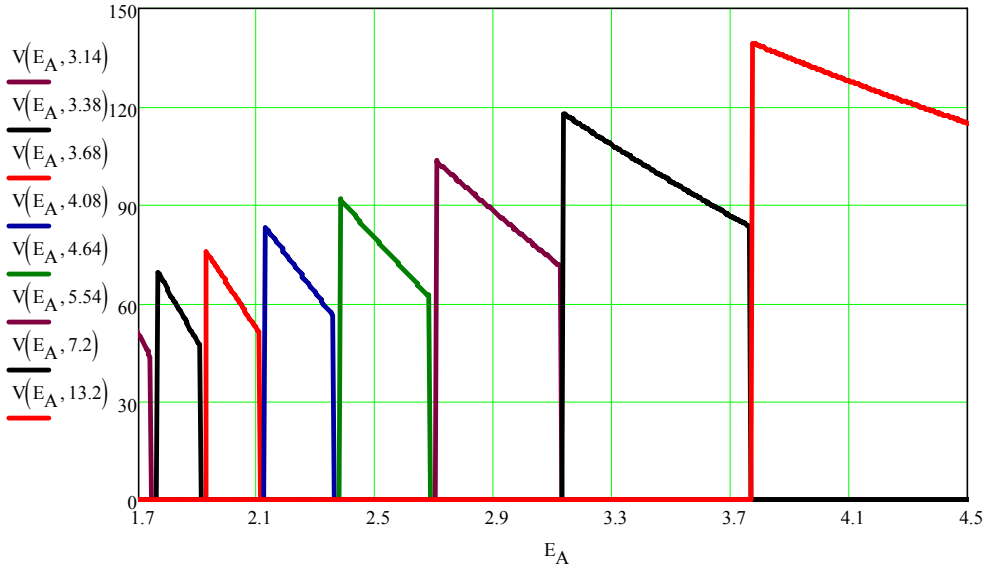

b)

Fig. 7.5. The function $V_{RF}(E_A, \gamma_{tr})$ at $\eta_\omega(E_A, \gamma_{tr})$ from the range 1 ÷ 4.5 GeV/u; the parameter γ_{tr} values are shown in the brackets of the function $V(E_A, \gamma_{tr})$. a) $1 < E_A < 1.7$ GeV/u, b) $1.7 < E_A < 4.5$ GeV/u,

These graphs show that variation of collider energy requires rather fine tuning of transition energy. Moreover, one needs to provide 16 (!) "machines" (lattice versions) at least.

One should note that the presented result can be optimized even more and number of "the machines" can be diminished. First of all, a significant simplification can be done if it would be possible to widen the $\eta_\omega(E_A)$ range (7.4) (by increase, for instance of bandwidth f_w).

8. Preliminary design of the twin bore SC magnets

The Nuclotron-type design based on a cold, window-frame iron yoke and a saddle-shaped winding of hollow superconductor [8.1] can be chosen for the collider. The preliminary design of the collider dipole magnet is shown in the Fig. 8.1. Two identical curved, single - layer windings are located in the common curved iron yoke one upon the other. Lorenz forces in the windings are supported by the yoke. The yoke consists of three parts made of laminated electrical steel 1 mm in thickness. They are held together by longitudinal steel plates welded with laminations and frontal sheets. The distance between the beams can be approximately 320 mm. The magnet is surrounded by a thermal shield and vacuum jacket (Fig. 8.2).

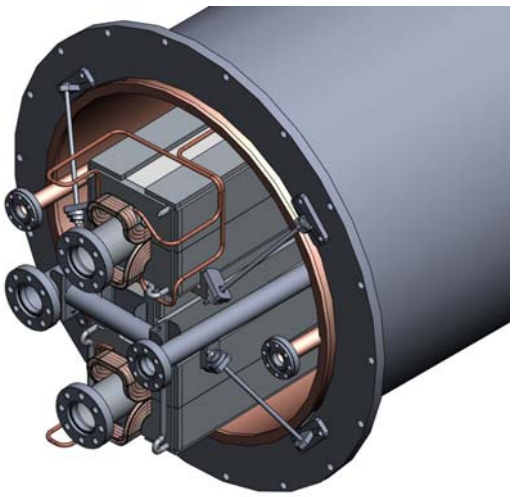

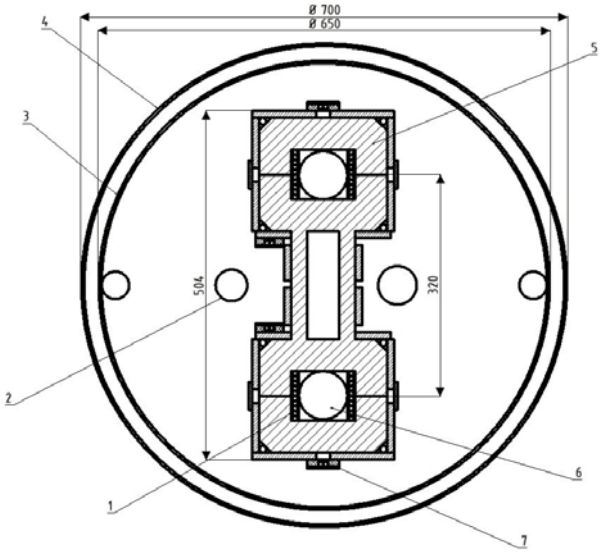

Fig. 8.1. Front view of the collider dipole magnet.

Fig. 8.2. Cross-sectional view of the dipole magnet: 1 – superconducting winding, 2 – supply helium header, 3 - thermal shield at the liquid nitrogen temperature, 4 – vacuum shell, 5 – iron yoke, 6 – beam pipe, 7 – bus bars.

The windings are made of a hollow superconducting cable. Sixteen SC strands are spirally wound on a copper-nickel tube 4 mm in diameter. The cable is wrapped with two layers of 0.04 mm Kapton tape and two layers of 0.1 mm epoxy impregnated glass-fiber tape. Wire and cable characteristics are presented in Fig. 8.3 and in Table 8.1.

The bending field in the iron-dominated magnets is limited by the value of about 2 T. The field geometry is formed by the iron yoke, therefore at the maximum field the relative imperfection is less than $6 \cdot 10^{-4}$. The winding current at the maximum field is designed to be 12 kA. The collider will be operated at constant magnetic field, but the power supply system is designed to provide maximum field ramp of 0.5 T/s. Design of the regular collider twin bore quadrupole lens with hyperbolic poles is in progress. The production, assembling, and cooling of the dipole and quadrupole magnets are similar. The main parameters of the dipole and quadrupole magnets are summarized in Table 8.2.

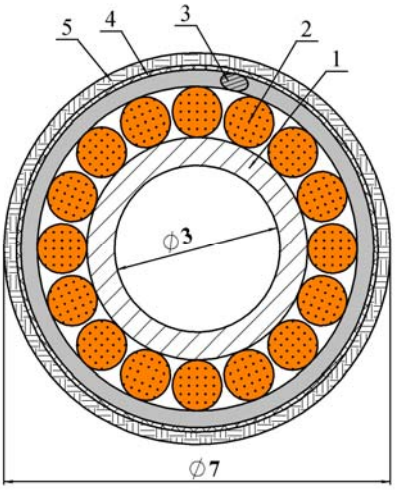

Fig. 8.3. Cross-sectional view of the cable: 1 - copper-nickel tube with channel for two-phase helium flow, 2- superconducting wire, 3 - nichrome wire, 4 – Kapton tape, 5 – glass-fiber tape.

Table 8.1. Wire and cable characteristics.

Wire	
Strand diameter, mm	0.9
Nb-Ti filament diameter, mcm	6
Filament twist pitch, mm	8
Copper to superconductor ratio	1.38
Critical current density for *Nb-Ti* at 2.5 T and 4.7 K, A/mm^2	3940
Cable	
Number of strands	16
Transposition pitch, mm	50
Cu-Ni tube outer diameter, mm	4
Cooling channel diameter, mm	3
Ni-Cr wire diameter, mm	0.3
Ni-Cr wire binding pitch, mm	0.6
Kapton insulating thickness, mcm	2 x 40
Glass- fiber tape thickness, mm	2 x 0.1
Cable diameter with insulation, mm	7.0
Operating current at 2.0T & 4.7K, kA	12
Critical current at 2.5 T & 4.7 K, A	16.8

Construction of the dipole magnet prototype is scheduled for 2010.

Table 8.2. The twin bore NICA Collider magnets parameters

Parameter	**Dipole**	**Quadrupole**
Number of magnets in the ring	64 + 1	32 + 2
Design: superferric; laminated cold iron yoke	Window-frame; curved	hyperbolic poles
Maximum magnetic induction (field gradient), T (T/m)	2.0	23
Effective magnetic length, m	2.2	0.52
Ramp rate dB/dt, T/s	≤ 0.5	-
Field quality $\Delta B/B$ ($\Delta G/G$)	$\pm 6 \cdot 10^{-4}$	
Useable aperture (beam pipe diameter), mm	70	70
Pole radius, m	-	0.036
Bending angle, deg	$5\,^{5}/_{8}$	-
Radius of curvature, m	22.5	-
Estimated yoke length, m	2.13	0.45
Yoke width, m	0.204	0.22
Yoke height, m	0. 504	0.52
Distance between the beams, mm	320	
Overall weight, kg	1200	230
Current at maximum field, kA	12	12
Number of turns in the winding (per pole)	10 (5)	4 (1)
Inductance, μH	370	22
Stored energy, kJ	26.6	1.58
Vacuum shell outer diameter, mm	700	
Vacuum shell length, m	1.8	0.7
Heat releases, W	10	4.8
SC cable cooling channel diameter, mm	3.0	3.0
Cable length in the two windings, m	110	14
Cable length in the bus bars, m	24	12
Pressure difference between the helium headers, kPa	27	
Maximal temperature of helium in the winding, K	4.65	

A helium flow - diagram of the collider magnet is presented in Fig. 8.4. The dipole and quadrupole magnets are cooled with a two-phase helium flow which in series passes from supply header through the cooling channels of the bus bars, lower and upper windings, iron yoke and then enters the return header. Each twin bore dipole or quadrupole magnet is connected in parallel to the supply and return helium headers. The mass vapor content of helium at the inlet is kept approximately equal to zero. Hydraulic resistance of cooling channels of magnets are adjusted so that the mass vapor content of helium at the outlet of the dipole and two type quadrupoles will be identical and equal 90%. In Table 8.3 is summarized the refrigeration capacity at 4.5 K needed for cooling the NICA collider magnets. Estimated value of total heat input to liquid helium in the collider is 960 W. Consumption of liquid helium for cooling the current leads is approximately 1.2 g/s.

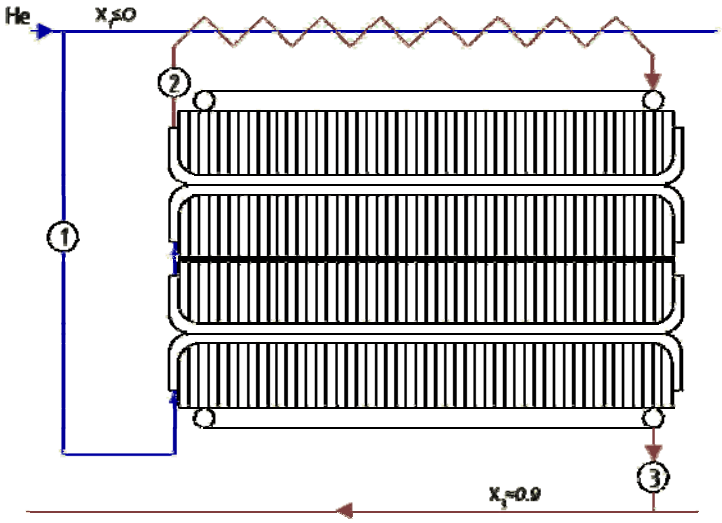

Fig. 8.4. Helium flow diagram of the magnet.

Table 8.3. The refrigeration capacity at 4.5 K needed for cooling the NICA collider magnets.

Heat leak to helium in the dipole magnets, W	650
Heat leak to helium in the quadrupole magnets, W	163
Heat leak to helium in the nonstructural elements, correction magnets, BPM, cold-warm transitions, measuring and voltage taps, etc., W	147
Total heat leak to helium in the collider, W	**960**
Consumption of liquid helium for cooling the current leads, g / s (l/hour)	**1.2** (35)

References

8.1. N.N. Agapov, A.M. Baldin, H.G. Khodzhibagiyan, A.D. Kovalenko, V.N. Kuzichev, V.A. Mikhailov, and A.A. Smirnov, «Low field cold iron SC-magnet technology: New aspects of application», *IEEE Trans. Appl. Supercond.*.vol. 10, N 1, pp.280-283, 2000.

9. Electron cooling and related problems

9.1. Luminosity evolution in time without cooling

Without a beam cooling, during the experiment the beam emittance and the bunch length increase due to intrabeam scattering (IBS) process. The expected horizontal IBS growth time values in the collider are of the order of 20 s at the 3.5 GeV/u ion energy. The bunches can be refreshed in the collider with periodicity determined by the beam preparation time, which is equal to 5.5 min. (one bunch per 5 s). In this case the average luminosity is about two times less than the peak one. Such a regime of the collider operation is acceptable; however it requires permanent work of the injection chain.

The situation can be significantly simplified by a beam cooling application during the experiment. In the equilibrium between the IBS and the cooling the luminosity life-time is limited mainly by the ion loss due to interaction with residual gas atoms. The vacuum conditions

in the collider rings are chosen to provide the beam life time of a few hours. In this case the average luminosity value is closed to the peak one. The collider rings are filled ones at the beginning of experiment and the beams have to be refreshed after a long time about 1 hour. Meanwhile the injection chain can be used for another experiments being performed in parallel.

In the required energy range the both electron and stochastic cooling method can be used. However there is a lack of the world experience presently of the cooling systems of required parameters. On one hand, the electron energy for the ion beam cooling at 3.5 GeV/u is equal to about 1.9 MeV (Table 9.1) that is much higher than in conventional electron cooling systems. Indeed, the highest energy of the electron beam reached in the Recycler cooling system (FNAL) is equal to about 4.3 MeV (that corresponds to the ion energy of about 8 GeV/u). Unfortunately this system is operated at low magnetic field value that does not allow to achieve short cooling time. The existing cooling systems with magnetized cooling are operated at the electron energy below 300 keV.

This investigation is dedicated to consideration and comparison of parameters of both possible cooling systems. The results of numerical simulations with the BETACOOL program are presented below. In these simulations the parameters of the ion beam (Table 9.1) were chosen according to the requirement of the collider luminosity of 1×10^{27} $cm^{-2}s^{-1}$.

Table 9.1. Ion beam parameters for colliding experiments

Energy, E, GeV/u	3.5
Ring circumference, C_{Ring}, m	336
Ion kind	$^{197}Au^{79+}$
Particle number per bunch, N_b	1×10^{9}
Bunch number, n	32
Unnormalized rms emittance, ε_b, π mm mrad	0.34
Momentum spread, σ_p	0.001
RMS bunch length, σ_s, cm	30
Beta function at collision point, β*, m	0.5
Harmonic number, h	160
Intrabeam scattering rates hor/ver/long, s^{-1}	0.055 / 0.0035 / 0.0105

The present version of the collider lattice is optimized for the equalization of the IBS heating rates over three dimensions. For the transverse degrees of freedom it was proposed that the collider is operated at coupling resonance and the heating rates in the horizontal and vertical planes are equal. At such condition, the initial values of the heating rates for the transverse and longitudinal degrees of freedom are equal to 0.03 and 0.01 s^{-1} correspondingly (Table 9.1).

During 200 seconds (which is equal to about $6\tau_{IBS}$) of the beam circulation in the ring the emittance increases by about 3 times (Fig.1, a) while the luminosity decreases by about 3 times (Fig.9.1, c). The bunch momentum spread increases by about 30% (Fig.9.1, b) that leads to corresponding increase of the bunch length. The role of the cooling application is to suppress both detrimental effects – the increase of the emittance and bunch length.

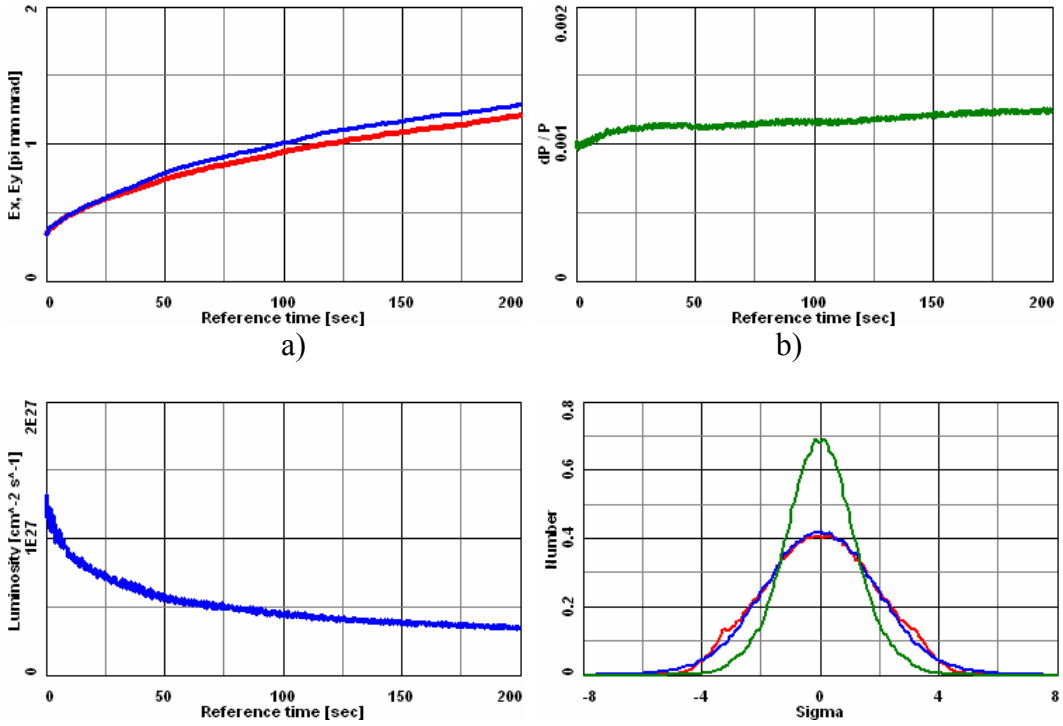

Fig.9.1. Evolution of the beam parameters without cooling.
a) rms transverse emittances, b) rms momentum spread, c) luminosity,
d) transverse (red, blue) and longitudinal (green) profiles after 200 seconds.

9.2. High energy electron cooler

High energy electron cooling was discussed since very beginning of the proposal of the method. Up to now the only electron cooling system was successfully constructed and put into operation in 2005. It is the electron cooling system of the electron energy of 4.3 MeV on the Recycler storage ring at FNAL. Its peculiarity is so called “non-magnetized” electron beam that is some disadvantage of the cooler. Two projects are under design presently: e-coolers with “magnetized” electron beam for HESR (FAIR/GSI), of electron energy up to 4.5 MeV, and for COSY (FZ-Juelich) of electron energy of 2 MeV. Parameters of the NICA electron cooler are very close to the COSY project.

The main function of the NICA electron cooler is to compensate an influence of the IBS heating (Table 9.1). Therewith, electron cooling is accompanied with parasitic process of electron-ion recombination in the cooling section. To diminish it we propose to use electron beam with artificially increased transverse temperature of electrons (by excitation of electron transverse velocities at the electron gun exit). Then, a “remedy” for providing of an efficient electron cooling with “hot” electron beam is required. This goal can be achieved with “magnetized cooling scheme”. In our cooler we plan to use high magnetic field - of 2 T (Table 9.2). This magnetic field will be provided with application of superconducting solenoids.

Electron energy is chosen to provide cooling in all ion energy range of 1 ÷ 4.5 GeV/u. Correspondingly, the maximum electron energy in e-cooler is of 2.47 MeV.

Table 9.2. Parameters of the NICA electron cooling system

Maximum electron energy, MeV	2.47
Effective cooler length, m	6.0
Electron beam current (max), A	0.5
Electron beam radius, cm	0.5
Magnetic field in cooling section, T	0.2 - 2.0
Magnetic field inhomogeneity in cooling section	2×10^{-5}
Beta functions in cooling section, m	20
Transverse electron temperature, eV	10.0
Longitudinal electron temperature, meV	5.0
Beam lifetime due to recombination, hour	2.0

Simulation of electron cooling process at cooler parameters demonstrates capability of the system to stabilize the luminosity at the required level during a long time (Fig. 9.2a). However, the electron cooling leads to formation of a dense core of the ion distribution function (Fig. 9.2b) that determines the luminosity level when very long tails of relatively low intensity are "out of the game". The tails are not stabilized by the cooling and their development can be one of probable channels of the ion loss. Another channel is the particle loss through recombination in the cooling section mentioned above. To suppress this process one needs to increase the electron temperature up to about 50 eV. Therefore, to keep sufficient value of the friction force the magnetic field in the cooling section has to be of the order of 2 T.

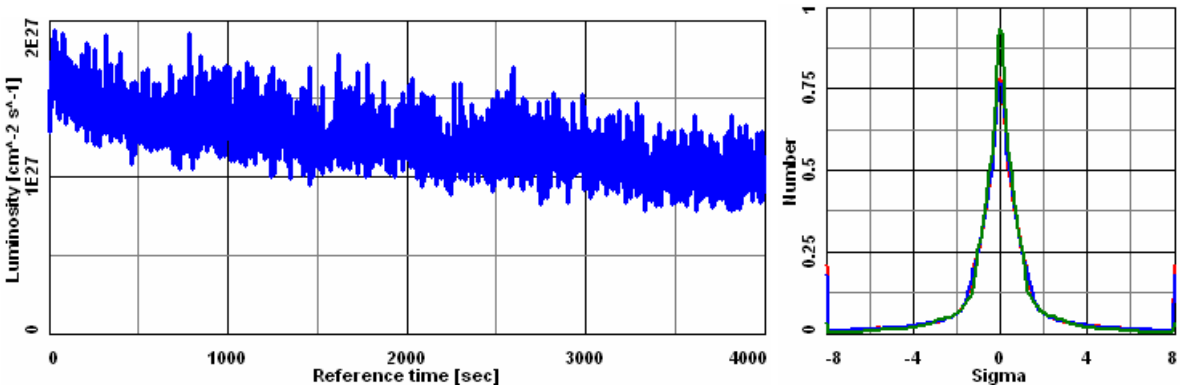

a) b)

Fig. 9.2. a) Luminosity variation during 1 hour of the experiment under electron cooling. b) The ion beam profile under the electron cooling after 4000 seconds. Vertical axis is the relative ion number, horizontal is the beam profiles in units of the initial r.m.s. value.

The main peculiarity of the proposed *e-cooler scheme* is location of two tubes in one high voltage tank –acceleration tube for the 1st ring and deceleration tube for 2nd one, and vice versa in another HV tank (Fig.9.3, 9.4).

Preliminary design of the collider electron cooling system was performed in co-operation with All-Russian Electrotechnical Institute (VEI, Moscow) on the basis of dynamitron-type high voltage generator (Fig.9.3). For the electron beam transport from the high-voltage vessels to the cooling section as well as for the cooling sections SC solenoids will be used. The electron beam transport inside the accelerating/decelerating columns is provided by SC solenoids placed outside of HV tanks (Fig.9.4a). Design of the high voltage generator prototype has been started; it will be constructed and tested by VEI.

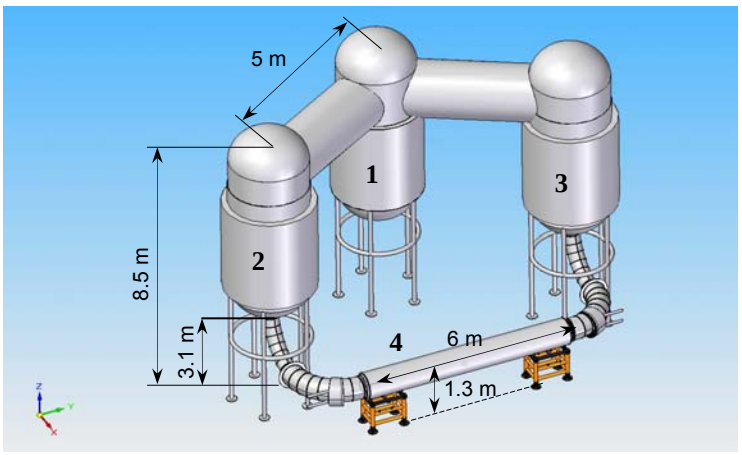

Fig.9.3. Electron cooling system of the collider:
1 – HV generator, 2, 3– HV tanks, 4 – cooling section.

Electron cooling system consists of the following main subsystems: electron beam formation system including electrostatic tubes, the electron gun and electron collector (Fig. 9.4b); magnetic system containing straight solenoid, toroidal solenoids, bending field coils for drift compensation in bending toroids, coils for the electron beam position correction; vacuum system that consists of vacuum chambers and vacuum pumps, as well as of tools for vacuum chamber heating and for pressure measurement; diagnostics system including two pairs of pickup stations at the entrance and the exit of the cooling section; nitrogen and helium cooling systems providing cooling of the SC solenoids, the collector, the electron gun anode and the radiators of air cooling and distillate water cleaning system; high voltage power supplies for electron gun and collector suspended to high potential; mechanical supports.

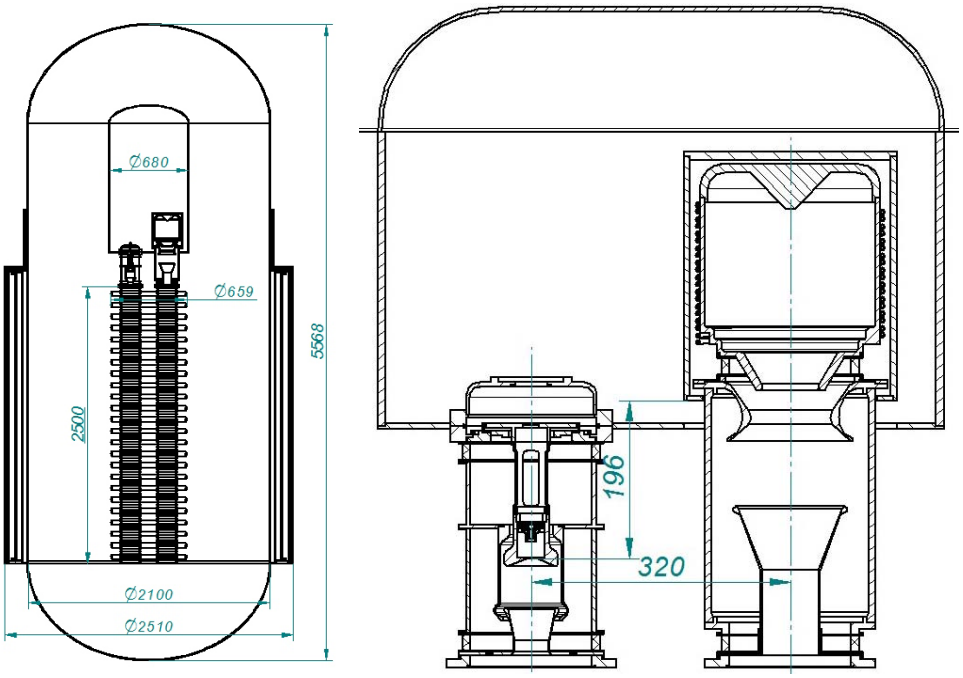

a) b)

Fig.9.4. a) High voltage tank with electron gun, electron collector and electrostatic tubes, SC solenoid in cryostat is shown schematically;
b) electron gun and electron collector of two beams of opposite directions.

Two pairs of dipole magnets will be installed in the cooler section for correction the ion beam trajectory displacement produced by vertical components of the electron cooler toroids field.

For simulation of the optics of the electron guns and electron collectors both BINP and JINR electron cooling groups use mostly the special code SAM developed in Budker INP. The code allows simulating the electron trajectories taking into account the geometry of electrodes, the longitudinal magnetic field, and the field of the electron beam space charge. As result of such simulation the profiles of electron gun electrodes of so called "adiabatic optics" has been found (Fig. 9.4b). The gun generates electron beam with optics "aberration" (additional transverse electron temperature) below 0.1 eV. Simulation of electron trajectories in the collector is in progress.

10. Vacuum system of the collider

Estimations of particle losses and transverse emittnace growth due to interaction with residual gas shows that the necessary static vacuum should be less then 5e-10 Torr in the warm equivalent and less then 1e-11 Torr for the helium temperature. The vacuum pressure in the isolation chamber is enough on the level of 1e-5 Torr. The main elements of the vacuum system are shown on the Fig.10.1.

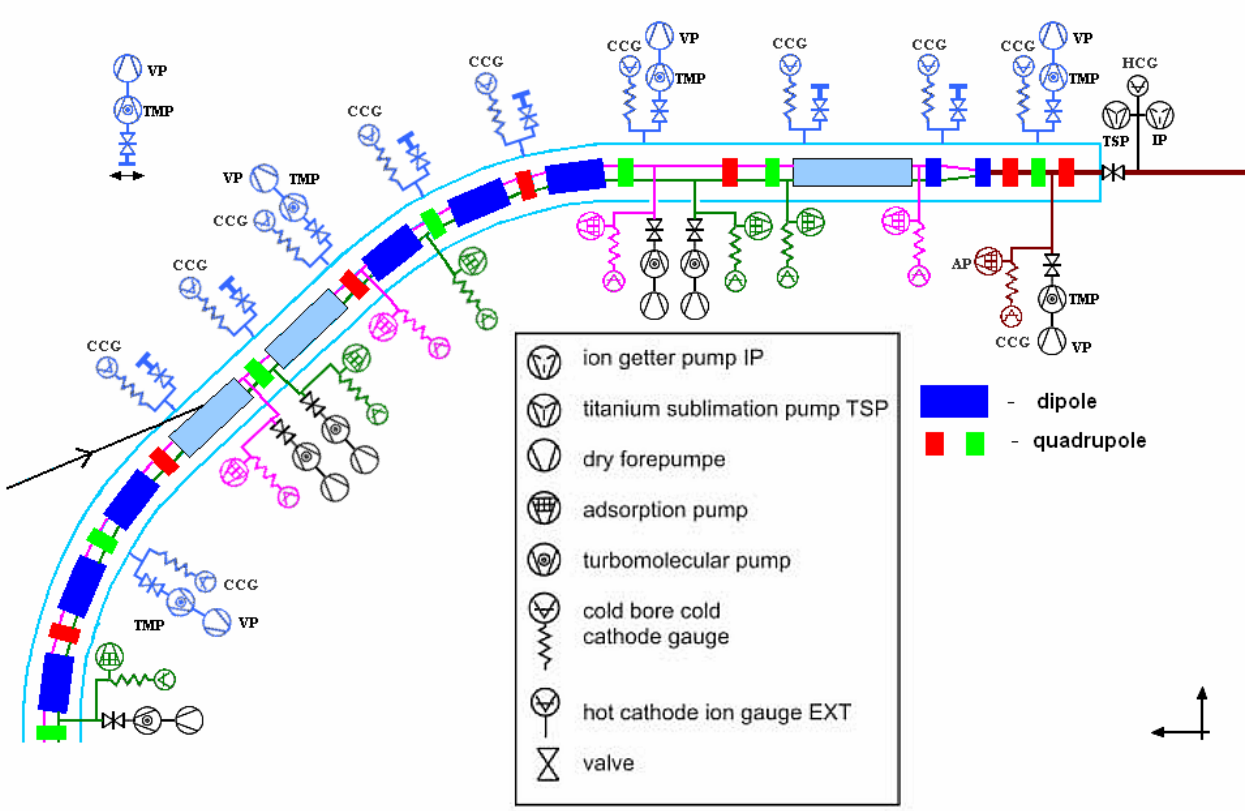

Fig.10.1. The vacuum system of collider ring (quarter of the ring).

11. Electron-Cloudless operation mode of the collider

The effect of electron clouds in NICA collider was analyzed first in 2008 at development of NICA CDR [11.1]. The simulation results were revised and renewed numbers are presented in this section. Both simulations were performed with ECLOUD code, version 3.3 [11.6].

Usually by *electron cloud effect* is meant so called *"beam induced multipacting"* – buildup of secondary electron avalanche ("*electron cloud*") in the electric field of particle bunches

circulating in a cyclic accelerator (collider) [11.2]. This effect leads to significant deterioration of vacuum in the accelerator and, as consequence, fast circulating beam particles loss. One should note that the *multipacting* phenomenon is well known in RF and microwave electronics where such an electron avalanche (discharge) is provoked by high frequency electric field.

The criteria for e-cloud formation can be formulated as the following ([11.2], [11.3]).
The necessary (or "resonance") condition:

$$(N_{bunch})_{necessary} > \beta^2 \cdot \frac{b^2}{Zr_e l_{space}} \quad . \tag{11.1}$$

Here N_{bunch} is ion number per bunch, βc is ion velocity, b is radius of vacuum chamber, Ze is ion charge, r_e is electron classic radius,

$$l_{space} = \frac{C_{Ring}}{n_{bunch}}$$

is interbunch distance, C_{Ring} is the ring circumference and n_{bunch} is bunch number.
The sufficient condition (acceleration of secondary electron in the bunch electric field up to "critical" energy):

$$(N_{bunch})_{sufficient} > \frac{\beta b^2}{Zr_e} \cdot \sqrt{\frac{E_{crit}}{2m_e c^2}} \quad . \tag{11.2}$$

Here the critical energy E_{crit} is secondary electron energy sufficient for kicking out the chamber wall more than one electron.

Another effect of electron cloud buildup can be storage of secondary electrons in ion bunch resulting that neutralizes bunch space charge and changes betatron tune shift [11.4]. This effect, as estimates show is more or less insignificant and we do now consider it here.

Secondary electron emission, as we see from consideration above, very critical phenomenon for electron clouds development and the value of secondary electron yield (SEY) is a critical parameter. Spectrum of secondary electrons – SEY dependence on energy – is very sensitive both to material of vacuum chamber wall and its conditioning. SEY data are available for pure metals (Fig. 11.2). Similar data for "*technical surfaces"* representative for vacuum chambers are quoted in Ref. 11.2. One can see that the SEY values for "technical" copper (Cu) and stainless steel (St) in Fig. 11.3 are slightly larger than for pure metals in Fig. 11.2.

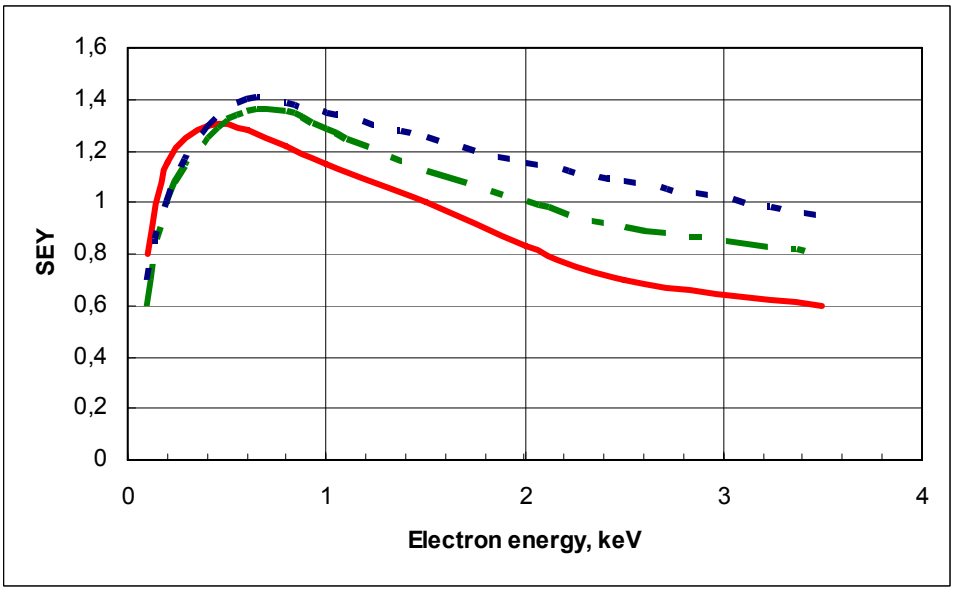

Fig. 11.2. Secondary electron yield vs primary electron energy for different materials: Fe - red solid line, Ni – green dash-dot line, Cu – blue dot line [11.5]

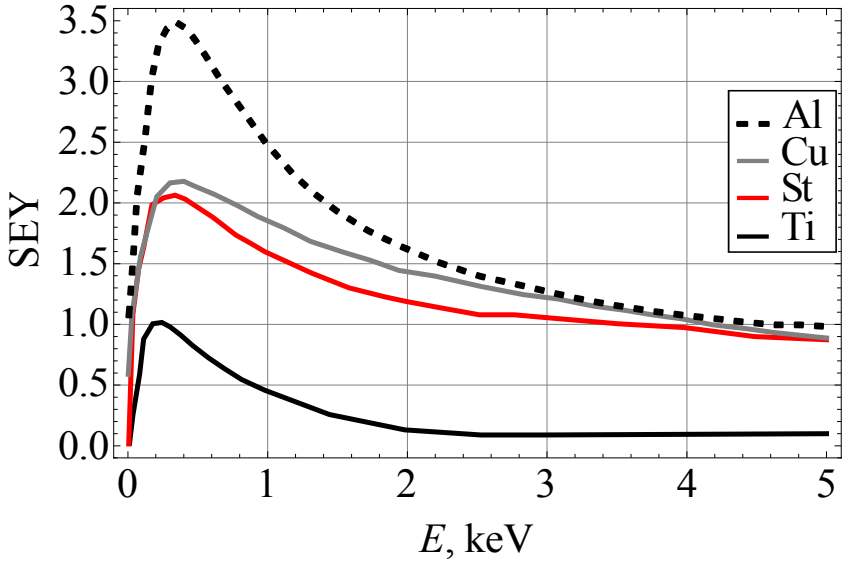

Fig. 11.3. Secondary electron yield vs primary electron energy for perpendicular incidence and for technical surfaces representative for vacuum chambers (extrapolated for $E > 2$ keV) [11.2]; materials: titanium (Ti), stainless steel (St), copper (Cu) and aluminum oxide Al_2O_3 (Al)

All these data are basic information for estimates of e-clouds effect development.

Substituting into criteria (11.1), (11.2) the NICA collider parameters (Tables 3.1, 4.1, 8.1)

$$\beta \approx 1,\ b = 3.5 \text{ cm},\ C_{Ring} = 336 \text{ m},\ n_{bunch} = 32,\ Z = 79,\ E_{crit} \sim 1 \text{ keV}$$

we find

$$(N_{bunch})_{necessary} = 7 \cdot 10^9,\ (N_{bunch})_{sufficient} = 1 \cdot 10^9.$$

Thus, such estimates show that NICA collider parameters are close to excitation of e-clouds development. Therefore numerical simulations have been fulfilled.

The simulation code

The preliminary estimates for e-cloud buildup for NICA was made using "ECLOUD code, version 3.2, 2005" developed by F. Zimmermann (see in [11.1]). Presently the new "version 3.3, 2009" of this code is available [11.6]. It gives rather good agreement with experimental results at SEY = 1.53 [11.7]. Therefore, the numerical simulations presented below were performed with this version of ECLOUD code.

Numerical simulations of electron clouds development in NICA collider

At simulations we used SEY coefficient for stainless steel from Fig. 11.3, red curve, and cross section of residual gas ionization by $^{197}Au^{79+}$ ions from Ref. 11.8. Other parameters are listed in Table 11.1.

Table 11.1. List of input parameters for e-cloud simulations

RMS beam emittance, π·mm·mrad	0.25
RMS bunch radius, mm	0.2
RMS bunch length, m	0.3
Dipole magnetic field, T	2.0
Vacuum chamber diameter $D_{chamber}$, mm	60/70/75
Residual gas pressure, Torr	$5 \cdot 10^{-11}$
Ionization cross section $\sigma(H_2)/\sigma(CO)$, $\times 10^{-15}$ cm^2	1.3/5.8

Special attention has been given to dipole sections, since in this case the conditions for e-cloud buildup more stringent compared with the straight sections.

Simulation results (Fig. 11.4) were obtained for the bunch spacing in the range of

3.58 m < S_b < 12.55 m, for δ_{max}= 1.5 and 5.02 m < S_b < 12.55 m, for δ_{max}= 2.

The electron-cloudless working modes of NICA collider is given in Fig. 11.4 below the blue curve. The instability threshold can be defined using ECLOUD code with some uncertainity (the program itself becomes "unstable"). Therefore the threshold is shown in Fig. 11.4 as a region marked in red and is bounded by two curves - blue and red ones.

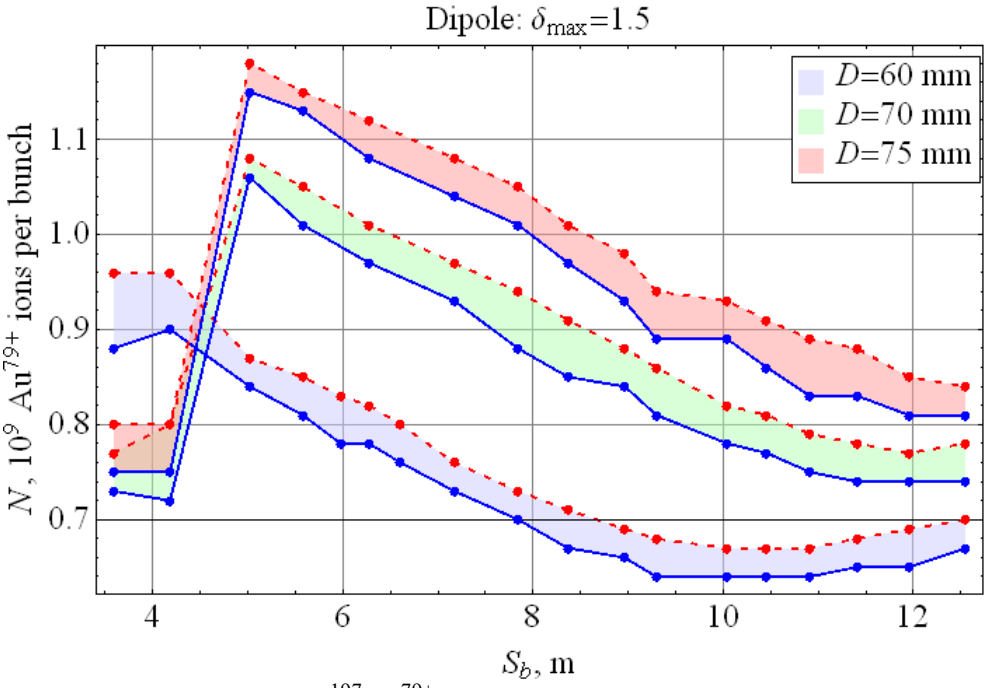

Fig. 11.4 a. Threshold values of $^{197}Au^{79+}$ ions per bunch vs bunch spacing S_b for δ_{max}= 1.5.

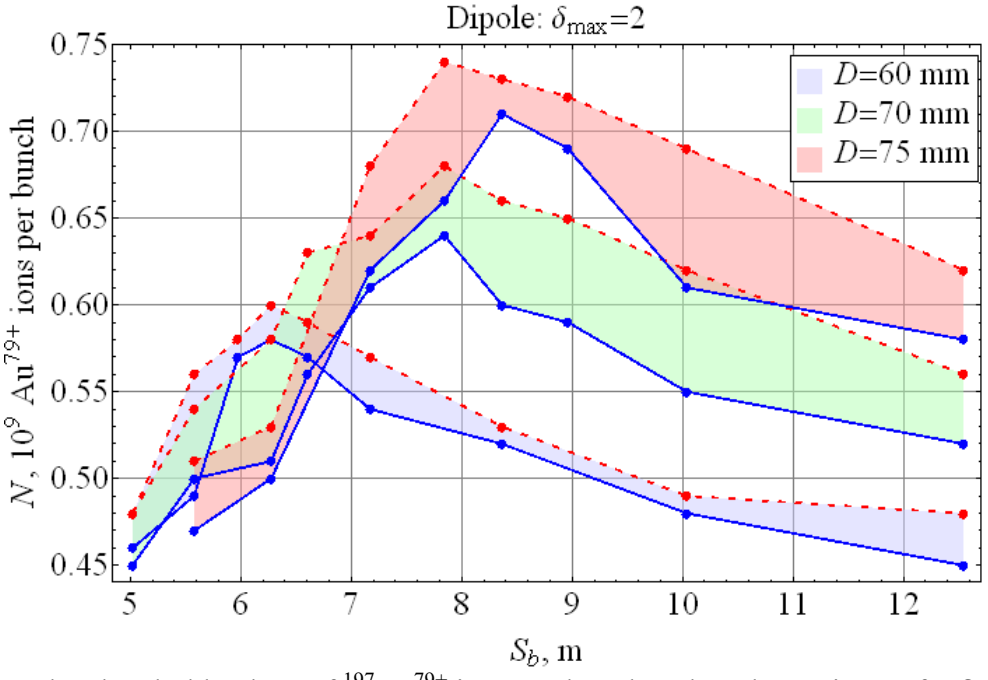

Fig. 11.4 b. Threshold values of $^{197}Au^{79+}$ ions per bunch vs bunch spacing S_b for δ_{max}= 2.

It is pertinent to note here that both pairs of the curves in Fig. 11.4 do demonstrate a resonance character of the N_{bunch} threshold dependence on S_b. That agrees qualitatively with consideration given above (Formulae 11.1, 11.2). However, the resonance width is very wide. This fact is connected with very wide dependence of SEY on primary electron energy (Fig. 11.2, 11.3). Indeed, the condition of resonance has to be written taking into account initial velocity of

secondary electrons and, correspondingly, all the spectrum of SEY. All such nuances are included as we can hope) in ECLOUD code.

Significant increase of the threshold ion number one can expect with reduction of SEY. For this purpose we began research on development of chamber wall coating with TiN.

References

11.1. Conceptual Design Report of Nuclotron-based Ion Collider fAcility (NICA), JINR, 2008
11.2. O. Gröbner, Beam induced multipacting,. Proc. of PAC'97, 1997, p.p. 3589–3591, (http://accelconf.web.cern.ch/accelconf/pac97/papers/pdf/4P004.PDF).
11.3. I.Meshkov, NICA Project Status, Report on Workshop "Physics of CBM" JINR, Dubna, May 19-22, 2009
11.4. P.Zenkevich, private communication (2009).
11.5. Physics Data, Handbook (in Russian), editors I.S.Grigoriev and E.Z.Melikhova, Energoatomizdat, 1991, p.584
11.6. http://proj-ecloud-code.web.cern.ch/proj-ecloud-code/default.htm.
11.7. G. Arduini, K. Cornelis, O. Gröbner, N. Hilleret, et al., Electron Cloud: Observations with LHC-Type Beams in the SPS,. Proc. of EPAC'2000, 2000, p.p. 939–941, (http://accelconf.web.cern.ch/accelconf/e00/PAPERS/THP1B16.pdf).
11.8. W. Fischer et al. Phys. Rev. ST Accel. Beams. 11. 041002. 2008.

12. Summary: collider parameters choice

First of all one has to formulate main limitations, which define the choice of collider parameters. The consideration done in preceding Chapters shows that as such *limitations* one can take the following effects.

1) Two Formulae - for collider luminosity (2.1) and for incoherent (Lasslet) tune shift (2.5) – can be considered as two equations for unknown variables. The solution of these equations gives us the required N_b and ε values for fixed L and ΔQ:

$$N_b \geq \frac{L}{|\Delta Q_{max}|} \cdot \frac{Z^2 r_p}{\beta^3 \gamma^3 A} \cdot \frac{C_{Ring}^2}{nc} \cdot \frac{\beta^*}{\sqrt{2\pi}\sigma_s} \cdot \frac{1}{f_{HG}\left(\frac{\sigma_s}{\beta^*}\right)}, \tag{12.1}$$

$$\varepsilon \leq \frac{L}{|\Delta Q_{max}|^2} \cdot \frac{Z^4 r_N^2}{4\pi\beta^5\gamma^6 A^2} \cdot \frac{C_{Ring}^3 \beta^*}{2\pi \cdot \sigma_s^2 nc} \cdot \frac{1}{f_{HG}(\frac{\sigma_s}{\beta^*})} . \tag{12.2}$$

Thus, we have found lower limit of N_b and upper limit of ε for given L and ΔQ.

2) *Keil-Schnell (KS) criterion* of the longitudinal microwave instability development[1]:

$$N_{KS} \leq 1.6 \cdot \frac{\beta^2 \gamma^3 A}{Z^2 r_N} \cdot \frac{\sigma_s \sigma_p^2 |\eta_\omega| \cdot F_L}{1 + 2 \cdot ln(b/a)} . \tag{4.8}$$

3) Beam-beam parameter

$$\xi = \frac{Z^2 r_p}{A} \frac{N_b}{4\pi\beta^2\gamma\varepsilon} \frac{1+\beta^2}{2}. \tag{2.7}$$

[1] For readers convenience we keep here the original numbers of the Formulae used in the preceding Chapters

4) Criterion defined by stochastic cooling application:

$$\eta_\omega(E_A) < \frac{f_s(E_A)}{6\sigma_p f_w} \quad . \tag{7.3}$$

5) RF voltage amplitude limitation:

$$V_{RF} = \frac{|\eta_\omega| \cdot \beta^2 \gamma}{2\pi h} \cdot \frac{A}{Z} \cdot \left(\frac{C_{Ring}}{\sigma_s} \cdot \sigma_p \right)^2 \cdot \frac{m_N c^2}{e} \le V_{max} \, . \tag{7.7}$$

These 5 criteria allow finding parameters values, which meet the main requirement – achievement of luminosity of $1 \cdot 10^{27}$ cm^{-2}·s^{-1} in all energy range.

As we can see from calculation results presented in Fig.12.1, 12.2, such a level of luminosity can be achieved at ΔQ = 0.05 and without violation of *KS criterion* if σ_s = 0.6 m if the ion number per bunch is varied with energy from $9 \cdot 10^9$ to $0.3 \cdot 10^9$ (thick solid blue curve in Fig. 12.1). Therewith beam emittance has to be varied with energy from 30 to 0.3 π·mm·mrad over all energy range (Fig.12.2, thick blue curve).

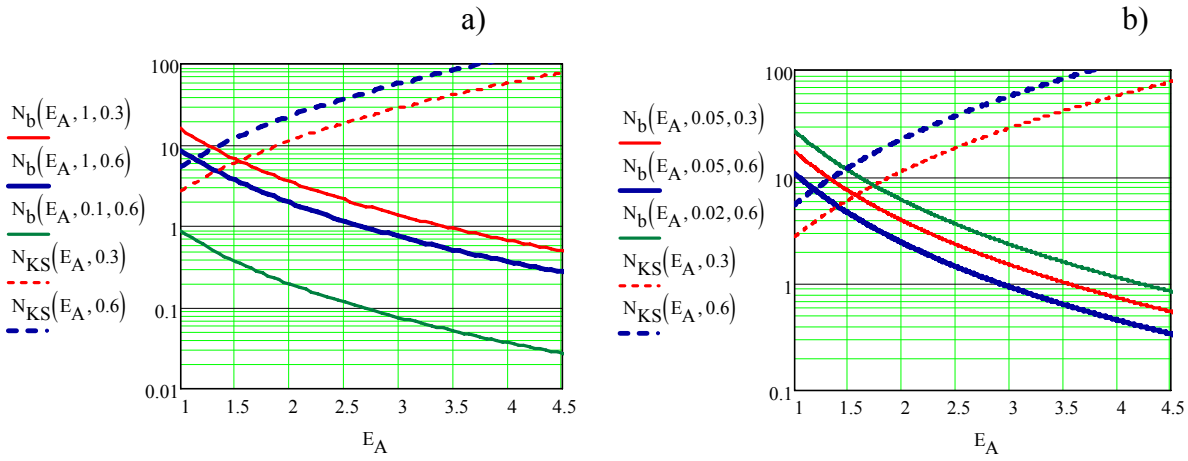

Fig.12.1. Ion number per bunch N_b (12.1) vs ion energy E_A [GeV/u] at different values of luminosity L, tune shift ΔQ and bunch r.m.s. length σ_s and *KS* criterion $N_{KS}(E_A, \sigma_s)$ (4.8) vs E_A.
N_b (three lower solid curves) and N_{KS} (two upper dash curves) in units of 10^9, L in 10^{27} cm^{-2}·s^{-1};
a) ΔQ = 0.05, parameters in brackets of N_b and N_{KS} functions: L = 1.0 and 0.1, σ_s = 0.3 and 0.6 m;
b) L = 1, parameters in brackets of N_b and N_{KS} functions: ΔQ = 0.05 and 0.02, σ_s = 0.3 and 0.6 m.

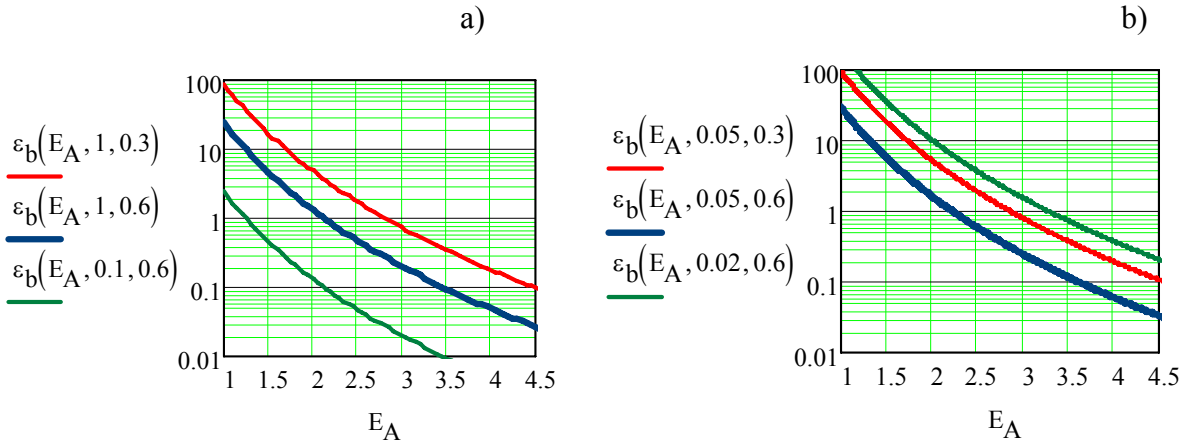

Fig.12.2. Beam emittance $\varepsilon_b(E_A, L, \sigma_s)$ (12.2) vs ion energy E_A [GeV/u] at different values of luminosity L and bunch r.m.s. length σ_s ;

ε_b in unit π·mm·mrad, L = (1.0 and 0.1)·10^{27} $cm^{-2}·s^{-1}$, σ_s = 0.3 and 0.6 m.

a) ΔQ = 0.05, parameters in brackets of $\varepsilon_b(E_A, L, \sigma_s)$ functions: L = 1.0 and 0.1, σ_s = 0.3 and 0.6 m;

b) L = 1, parameters in brackets of $\varepsilon_b(E_A, \Delta Q, \sigma_s)$ functions: ΔQ = 0.05 and 0.02, σ_s = 0.3 and 0.6 m.

Simultaneously, the *beam-beam parameter* remains sufficiently small in all energy range (Fig. 12.3).

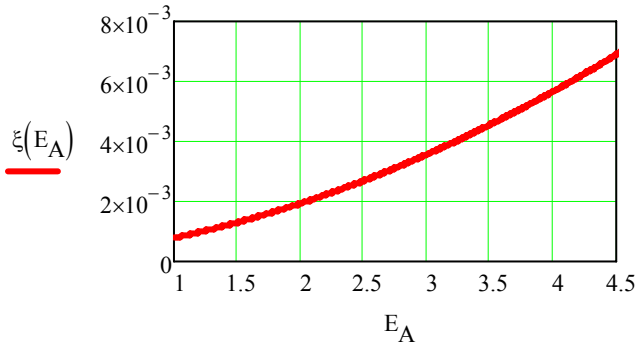

Fig. 12.3. Beam-beam parameter ξ vs ion energy E_A at ΔQ = 0.05 σ_s = 0.6 m when other parameters have values plotted in Fig. 12.1 and 12.2 at L = 1e27 $cm^{-2}·s^{-1}$.

The problem of the *slippage factor* and *RF voltage* is discussed in Chapter 7, where we have found rather strict requirements to ring lattice tuning.

A serious question remains to be answered:
Is electron or/and stochastic cooling capable to form and keep the beam with parameters shown in Fig. 12.1, 12.2, i.e. to suppress IBS in such an intense ion beam of very small emittance? Analysis of this problem is in progress.

Another problem appears at low ion energy: a necessity to store a large number of ions. This is possible (in principle) when application of barrier bucket stacking is foreseen (Chapter 5). However, the stacking time grows up by one order of magnitude!

Concluding we list the main collider parameters (Table 12.1)

Table 12.1. The main collider parameters

Ion energy range, GeV/u	1 ÷ 4.5
Ring circumference, m	336
Luminosity, $cm^{-2} \cdot s^{-1}$	$1 \cdot 10^{27}$
Lasslett tune shift (2.5)	0.05
Ion number per bunch	(9 ÷ 0.3)e9
Rms unnormalized beam emittance π·mm·mrad	30.0 ÷ 0.03
Rms momentum spread σ_p	1e-3
Rms bunch length σ_s, m	0.6
Transition energy GeV/u	3.2 ÷ 14.2 (16 “machines”)
Number of bunches	32
Number of RF harmonics	160
Beam-beam parameter (2.7)	(1 ÷ 7)e-3